arXiv:2104.07263v2 [math.NA] 6 Sep 2022

MULTI-INDEX ENSEMBLE KALMAN FILTERING

HÅKON HOEL, GAUKHAR SHAIMERDENOVA*, AND RAÚL TEMPONE

Abstract. In this work we combine ideas from multi-index Monte Carlo and ensemble Kalman filtering (EnKF) to produce a highly efficient filtering method called multi-index EnKF (MIEnKF). MIEnKF is based on independent samples of four-coupled EnKF estimators on a multi-index hierarchy of resolution levels, and it may be viewed as an extension of the multilevel EnKF (MLEnKF) method developed by the same authors in 2020. Multi-index here refers to a two-index method, consisting of a hierarchy of EnKF estimators that are coupled in two degrees of freedom: time discretization and ensemble size. Under certain assumptions, when strong coupling between solutions on neighboring numerical resolutions is attainable, the MIEnKF method is proven to be more tractable than EnKF and MLEnKF. Said efficiency gains are also verified numerically in a series of test problems.

Key words: Monte Carlo, multilevel, multi-index, convergence rates, Kalman filter, ensemble Kalman filter
AMS subject classification: 65C30, 65Y20.

1. Introduction

The ensemble Kalman filter (EnKF) is a widely used data assimilation method for high-dimensional state-space problems with nonlinear dynamics. Owing to its simple implementation and efficiency, ensemble-based filtering methods have rapidly gained popularity in geophysical sciences with applications, for example, in weather forecasting [40], atmosphere-ocean/lake simulations [37, 7, 31], and oil reservoir management [1, 56]. The EnKF method was originally proposed by Evensen [20]. Subsequently, several variants were developed [36, 15, 3]. EnKF approximates the filtering distribution using the empirical measure of its ensemble members. The L^p-convergence of the EnKF method with perturbed observations [36] has been studied in the literature [49, 46].

A considerable challenge in numerical filtering methods is the increase in simulation cost as the numerical resolution gets finer. This challenge can be overcome by the multilevel Monte Carlo method (MLMC) [24], which achieves substantial variance reduction by simulating pairwise coupled realizations on a hierarchy of temporal discretization levels. MLMC is a flexible methodology that has been combined with many other methods and successfully implemented in various fields: quasi-Monte Carlo [25, 43, 55], sequential Monte Carlo [13, 12, 51, 44], inverse problems and experimental design [10, 57, 47, 26, 58], differential equations with randomness [39, 19, 8, 42, 9, 5], limit theorems [2, 33], importance sampling [32, 41, 21], and machine learning [48].

© 2022. This manuscript version is made available under the CC-BY-NC-ND 4.0 license https://creativecommons.org/licenses/by-nc-nd/4.0/.

*Corresponding author: G.Shaimerdenova (gaukhar.shaimerdenova@kaust.edu.sa).

The multilevel EnKF (MLEnKF) method was introduced by Hoel et al. [34] for stochastic differential equation models with discrete-time observations, and an alternative version based on a sample average of independent pairwise coupled EnKF estimators was subsequently developed [35]. The main difference between these two versions of MLEnKF is that [34] uses one universal Kalman gain to update the ensemble members on all hierarchy levels, while [35] employs one Kalman gain per independent EnKF sample in the full MLEnKF estimator. The latter approach introduces less correlation between all particle members of the MLEnKF estimator, which particularly simplifies convergence analysis and paves the way for extending MLEnKF to the multi-index EnKF (MIEnKF) method introduced in this work. The MLEnKF method was extended to spatiotemporal (infinite-dimensional state space) models [17]. Similar multilevel techniques have been combined with other ensemble-based filtering methods, such as particle filters [38, 6], transform particle filters [28, 27], multigrid [50] and the recent extension to the continuous-time (Kalman–Bucy) filter [16].

The successful implementation of MLMC depends on a strong pairwise coupling between realizations on neighboring hierarchy levels, meaning a coupling that leads to substantial variance reduction. For stochastic differential equations with sufficiently smooth coefficients, this is achieved quite easily, but in more realistic problems with low-regularity features this can be extremely challenging if at all possible. See [22] for multilevel data assimilation applied to reservoir history matching, and [23, 53, 54] for applications of MLEnKF using sampling resolution constraints (so-called multi-fidelity methods).

Another important method is the multi-index Monte Carlo method (MIMC) [29], which forms the basis of this work. MIMC consists of a multi-index hierarchy of coupled realizations on neighboring resolutions, and can be regarded as an extension of MLMC. Many concepts related to particle-wise coupling in the proposed MIEnKF method are common in the MIMC method for McKean-Vlasov dynamics [30].

The contributions of this work are to develop the MIEnKF method with a subtle variance-reducing coupling idea for realizations on neighboring resolutions, and to numerically verify the asymptotic efficiency gains that MIEnKF achieves over EnKF and MLEnKF. The MIEnKF method extends the recent MLEnKF method [35] by treating not only the numerical discretization but also the EnKF ensemble size as degrees of freedom – resolution parameters. MIEnKF introduces a four-coupling of EnKF estimators (i.e., a coupling in both degrees of freedom) that produces a stronger variance reduction than the pairwise coupling in MLEnKF. Under certain assumptions, MIEnKF is also shown theoretically to achieve efficiency gains over counterparts for weak approximations of quantities of interest (QoI) in the classic and more robust setting of $\alpha = 1$ and $\beta = 2$ defined in [35], cf. Table 1.

Methods	EnKF	MLEnKF	MIEnKF
Mean-squared error	$\mathcal{O}(\epsilon^2)$	$\mathcal{O}(\epsilon^2)$	$\mathcal{O}(\epsilon^2)$
Computational cost	$\mathcal{O}(\epsilon^{-3})$	$\mathcal{O}(\epsilon^{-2}\,\lvert\log(\epsilon)\rvert^3)$	$\mathcal{O}(\epsilon^{-2})$

TABLE 1. Comparison of computational costs versus errors for ensemble Kalman filtering (EnKF), multilevel EnKF (MLEnKF) and multi-index EnKF (MIEnKF) methods, cf. Section 4.

The rest of this work is organized as follows. In Section 2, the setting and notation for filtering problem are introduced and a brief overview of the EnKF, mean-field EnKF (MFEnKF), and MLEnKF methods is presented. Section 3 describes the framework of the MIEnKF method. Section 4 presents theory on the performance of the MIEnKF method, including a theorem on approximation error versus computational cost. Section 5 compare the performance of MIEnKF to MLEnKF and EnKF in a series of numerical examples, and we wrap up with concluding remarks in Section 6.

2. Problem setting

In this section, we introduce the filtering problem of interest and give a brief overview of relevant ensemble-based filtering methods.

Let $(\Omega, \mathcal{F}, \mathbb{P}; \{\mathcal{F}_t\}_{t\geq 0})$ be a complete probability space equipped with a filtration $\{\mathcal{F}_t\}_{t\geq 0}$ of sub-σ-algebras of $\mathcal{F} = \mathcal{F}_\infty$. We denote by $L_t^p(\Omega, \mathbb{R}^k)$ the space of $\mathcal{F}_t\backslash\mathcal{B}^k$-measurable functions[1] $u : \Omega \to \mathbb{R}^k$ with $\mathbb{E}\left[|u|^p\right] < \infty$. Given the initial value $u_0 \in \cap_{p\geq 2} L_0^p(\Omega, \mathbb{R}^d)$, we consider the discrete-time filtering problem for a system of stochastic dynamics defined by a sequence of random maps $\Psi_n : \mathbb{R}^d \times \Omega \to \mathbb{R}^d$ and observations with additive noise:

$$\begin{cases} u_{n+1}(\omega) = \Psi_n(u_n, \omega), \\ y_{n+1}(\omega) = H u_{n+1}(\omega) + \eta_{n+1}, \end{cases}$$

where $\omega \in \Omega$, $n \in \mathbb{N}_0 := \mathbb{N} \cup \{0\}$, $H \in \mathbb{R}^{m\times d}$ is an observation operator, $\{\eta_k\}_{k\in\mathbb{N}}$ is an independent and identically distributed (i.i.d.) sequence with $\eta_1 \sim N(0, \Gamma)$ and with the independence property $\{\eta_k\}_{k\in\mathbb{N}} \perp \{u_k\}_{k\in\mathbb{N}_0}$. When confusion is not possible, we shall not indicate the dependence on ω for random variables.

Let $Y_n := (y_1, y_2, ..., y_n)$ denote the accumulated observation data up to time n using the convention that $Y_0 := \emptyset$. The main objective of a filtering method is to track the underlying signal u_n given Y_n through computing the conditional distribution of u_n give Y_n. The exact filter density for this problem – the so-called Bayes filter – satisfies the following iterative equations:

$$\textbf{Prediction} \quad \rho_{u_n|Y_{n-1}}(u) \propto \int_{\mathbb{R}^d} \rho_{u_n|u_{n-1}}(u)\rho_{u_{n-1}|Y_{n-1}}(v)dv$$

$$\textbf{Update} \quad \rho_{u_n|Y_n}(u) \propto \exp\left(-\left|\Gamma^{-1/2}(y_n - Hu)\right|^2/2\right)\rho_{u_n|Y_{n-1}}(u).$$

We will refer to the posterior distribution in the above update step as the true filter. In the linear-Gaussian setting, the Kalman filter is an exact algorithm that tracks the mean and covariance of the true filter. When Ψ is nonlinear the true filter becomes non-Gaussian, and the Kalman filter does not apply anymore. Therefore, approximation methods are needed. Among such, particle filters converge to the true filter in the large particle limit, but they are conjectured to perform poorly in high dimensions [11]. The EnKF performs more robustly than particle filters in high dimensions, but it has poorer convergence properties. In the large-ensemble limit, EnKF converges to the so-called mean-field EnKF in the large-ensemble limit [46, 35]. However, due to the application of a biased Gaussian ansatz in the update step of EnKF [20], the mean-field EnKF is not equal to the true filter in nonlinear problem settings. Despite this disparity, the EnKF is a robust and efficient method

[1]The function u is $\mathcal{F}_t\backslash\mathcal{B}^k$-measurable iff $u^{-1}(B) \in \mathcal{F}_t$ for all $B \in \mathcal{B}^k$, where $\mathcal{B}^k$ denotes the Borel σ-algebra on $\mathbb{R}^k$.

that is popular approach among practitioners. Connections between the mean-field EnKF and the true filter are discussed in [45, 35], but there are many open questions that remain to be studied, such as the convergence properties of EnKF in the large-ensemble and long-time limit.

The main objective of this paper is to construct an efficient MIEnKF method that converges weakly to the mean-field EnKF in the large-ensemble limit. In other words, for a given QoI $\varphi : \mathbb{R}^d \to \mathbb{R}$, our method approximates

$$\mathbb{E}^{\bar{\mu}_n}[\varphi(u)] = \int_{\mathbb{R}^d} \varphi(u)\bar{\mu}_n(du),$$

where $\bar{\mu}_n$ denotes the mean-field EnKF measure at time n, cf. Section 2.2.

Notation.

- *For $f, g : (0,\infty) \to [0,\infty)$ the notation $f \lesssim g$ implies that there exists a $C > 0$ such that*
$$f(x) \leq Cg(x), \quad \forall x \in (0,\infty).$$
- *The notation $f \eqsim g$ implies that $f \lesssim g$ and $g \lesssim f$.*
- *The expectation operator is defined by $\mathbb{E}[\cdot]$ and the variance operator (applicable to scalar-valued rv) is denoted by $\mathbb{V}[\cdot]$.*
- *For $d \in \mathbb{N}$, $|x|$ denotes the Euclidean norm of a vector $x \in \mathbb{R}^d$. For $\mathcal{F}\backslash\mathcal{B}^d$-measurable functions $u : \Omega \to \mathbb{R}^d$ and $p \geq 1$,*
$$\|u\|_p := \|u\|_{L^p(\Omega,\mathbb{R}^d)} = \left(\int_\Omega |u(\omega)|^p \, \mathbb{P}(d\omega)\right)^{1/p}.$$
- $\lceil x \rceil := \min\{z \in \mathbb{Z} \mid z \geq x\}$.

Let Ψ_n^N denote the numerical discretization of the dynamics Ψ_n using $N \geq 1$ uniform timesteps over every observation-time interval. The following assumption ensures that the mean-field EnKF measure $\bar{\mu}_n$ is well-defined cf. [35, Appendix A] and Section 2.2:

Assumption 1. Let $u, v \in \cap_{p\geq 2} L_n^p(\Omega, \mathbb{R}^d)$ for any $n \in \mathbb{N}_0$, $p \geq 2$, then there exists a constant $c_p > 0$ such that for all $N \geq 1$:

(i) $\left\|\Psi_n^N(u)\right\|_p \leq c_p(1 + \|u\|_p)$,
(ii) $\left\|\Psi_n^N(u) - \Psi_n^N(v)\right\|_p < c_p \|u - v\|_p$.

2.1. **EnKF.** The EnKF method is an ensemble-based nonlinear filtering method that is an extension of the Kalman filter. For an EnKF ensemble of size P, let $v_{n,i} := v_n(\omega_i)$ and $\hat{v}_{n,i} := \hat{v}_n(\omega_i)$, respectively, denote the $i-$th particle of the prediction and updated ensemble at time n. Then, the EnKF algorithm with perturbed observations and numerical dynamics Ψ^N comprises the following steps:

$$(1) \quad \textbf{Prediction} \begin{cases} v_{n+1,i} = \Psi_n^N(\hat{v}_{n,i}), \quad i = 1, 2, ..., P, \\ m_{n+1} = \dfrac{1}{P}\displaystyle\sum_{i=1}^P v_{n+1,i}, \\ C_{n+1} = \dfrac{1}{P-1}\displaystyle\sum_{i=1}^P (v_{n+1,i} - m_{n+1})(v_{n+1,i} - m_{n+1})^{\mathbf{T}}. \end{cases}$$

$$\textbf{Update} \quad \begin{cases} \tilde{y}_{n+1,i} = y_{n+1} + \eta_{n+1,i}, \quad i = 1, 2, ..., P, \\ K_{n+1} = C_{n+1} H^{\mathbf{T}} (H C_{n+1} H^{\mathbf{T}} + \Gamma)^{-1}, \\ \hat{v}_{n+1,i} = (I - K_{n+1} H) v_{n+1,i} + K_{n+1} \tilde{y}_{n+1,i}, \end{cases} \tag{2}$$

where $\eta_{n+1,i}$ are i.i.d. draws from $N(0, \Gamma)$.

The updated EnKF empirical measure is defined by

$$\mu_n^{N,P}(dv) = \frac{1}{P} \sum_{i=1}^{P} \delta(dv; \hat{v}_{n,i}),$$

where δ is the Dirac measure centered at $\hat{v}_{n,i}$, and the expectation of a QoI $\varphi : \mathbb{R}^d \to \mathbb{R}$ with respect to the EnKF empirical measure is expressed as

$$\mu_n^{N,P}[\varphi] = \frac{1}{P} \sum_{i=1}^{P} \varphi(\hat{v}_{n,i}). \tag{3}$$

Note that $\mu_n^{N,P}[\varphi]$ is a random variable that depends on parameters N and P. Under sufficient regularity, $\mu_n^{N,P}[\varphi] \to \bar{\mu}_n[\varphi]$ as $N, P \to \infty$, cf. [46, 35, 17], where $\bar{\mu}_n[\varphi]$ denotes the expectation of φ with respect to the mean-field EnKF measure that is introduced in the next section.

2.2. **MFEnKF.** The MFEnKF is the large-ensemble and fine-discretization limit of EnKF. In the large-ensemble limit, the Kalman gain becomes a deterministic matrix. Consequently, one may view MFEnKF as an ensemble of i.i.d. noninteracting particles, so that it suffices to represent the resulting filtering distribution by one particle. Let $\bar{v}_n$ and $\hat{\bar{v}}_n$ denote the prediction and updated state of a mean-field particle at time n, respectively. The following algorithm defines the MFEnKF for fully non-Gaussian models:

$$\textbf{Prediction} \quad \begin{cases} \bar{v}_{n+1} = \Psi_n(\hat{\bar{v}}_n) \\ \bar{m}_{n+1} = \mathbb{E}\left[\hat{\bar{v}}_{n+1}\right], \\ \bar{C}_{n+1} = \mathbb{E}\left[\left(\hat{\bar{v}}_{n+1} - \bar{m}_{n+1}\right)\left(\hat{\bar{v}}_{n+1} - \bar{m}_{n+1}\right)^{\mathbf{T}}\right]. \end{cases}$$

$$\textbf{Update} \quad \begin{cases} \tilde{y}_{n+1} = y_{n+1} + \tilde{\eta}_{n+1}, \\ \bar{K}_{n+1} = \bar{C}_{n+1} H^{\mathbf{T}} (H \bar{C}_{n+1} H^{\mathbf{T}} + \Gamma)^{-1}, \\ \hat{\bar{v}}_{n+1,i} = (I - \bar{K}_{n+1} H) \hat{\bar{v}}_{n+1,i} + \bar{K}_{n+1} \tilde{y}_{n+1,i}, \end{cases}$$

where $\tilde{\eta}_{n+1}$ is i.i.d. draws from $N(0, \Gamma)$.

The expectation of a QoI $\varphi : \mathbb{R}^d \to \mathbb{R}$ with respect to the updated mean-field EnKF measure is given by

$$\bar{\mu}_n[\varphi] := \mathbb{E}^{\bar{\mu}_n}[\varphi(v)] = \int_{\mathbb{R}^d} \varphi(v) \bar{\mu}_n(dv).$$

Remark 1. For the EnKF filter with the numerical-solution dynamics Ψ_n^N (instead of Ψ), Assumption 1 ensures that the analogous mean-field EnKF measure $\bar{\mu}_n^N$ is well-defined for any observation time $n \geq 0$ and numerical resolution $N \geq 1$, cf. [35, Appendix A].

2.3. **MLEnKF.** The recently developed MLEnKF method [35] is a natural stepping stone on the way from EnKF to explaining all of the complexities in the MIEnKF method. MLEnKF is a filtering method based on a sample average of independent and pairwise coupled samples of EnKF estimators at different resolution levels.

Let $L \in \mathbb{N}$ denote the finest resolution level of the estimator, and let the sequences

$$N_\ell = N_0 \times 2^\ell \quad \text{and} \quad P_\ell = P_0 \times 2^\ell \quad \text{with} \quad N_0, P_0 \in \mathbb{N}, \quad \ell = 0, 1, \ldots, L$$

respectively denote the numerical resolution and ensemble size.

Pairwise coupling of EnKF estimators. For a level $\ell \geq 0$, let

$$\hat{v}^\ell_{n,i} := \hat{v}^\ell_n(\omega^\ell_i) \qquad i = 1, \ldots, P_\ell$$

denote $i-$th particle of the updated ensemble at time n in size P_ℓ corresponding to the fine-level numerical resolution N_ℓ. Each $\hat{v}^\ell_{n,i}$ is *coupled pairwise* to the respective $i-$th particle of the coarser-level updated ensemble at time n computed with the numerical resolution $N_{\ell-1}$ via shared driving noise ω^ℓ_i. To obtain a $1 \leftrightarrow 1$ coupling between ensemble-members/particles on the fine- and coarse level, the total size of the coarse-level ensemble is set to P_ℓ with the relation $P_\ell = 2P_{\ell-1}$, meaning that the coarse-level ensemble can be viewed as a union of two ensembles in size $P_{\ell-1}$:

$$\hat{v}^{\ell-1,1}_{n,i} := \hat{v}^{\ell-1,1}_n(\omega^\ell_i) \qquad i = 1, \ldots, P_{\ell-1}$$

and

$$\hat{v}^{\ell-1,2}_{n,i} := \hat{v}^{\ell-1,2}_n(\omega^\ell_{P_{\ell-1}+i}) \qquad i = 1, \ldots, P_{\ell-1},$$

with the convention $\hat{v}^{-1,\cdot} := 0$.

It is important to note here that the particle-wise pairs share the same realization of driving noise within a level and the superscript ℓ in ω^ℓ_i indicates an independence of underlying noise between levels. In addition to this, the pairwise coupling is imposed under the particle-wisely shared initial condition:

$$\hat{v}^\ell_{0,i} = \begin{cases} \hat{v}^{\ell-1,1}_{0,i} & \text{if} \quad i \in \{1, \ldots, P_{\ell-1}\} \\ \hat{v}^{\ell-1,2}_{0,i-P_{\ell-1}} & \text{if} \quad i \in \{P_{\ell-1}+1, \ldots, P_\ell\}, \end{cases}$$

and the perturbed observations are also shared particle-wisely (see the below update step). Iterative simulation of pairwise coupled ensemble-members on the ℓ-th resolution level of the MLEnKF filter consists of the following prediction and update steps:

$$\text{(4)} \qquad \textbf{Prediction} \begin{cases} v^{\ell-1,1}_{n+1,i} = \Psi^{N_{\ell-1}}_n(\hat{v}^{\ell-1,1}_{n,i}), & i = 1, \ldots, P_{\ell-1}, \\ v^{\ell-1,2}_{n+1,i} = \Psi^{N_{\ell-1}}_n(\hat{v}^{\ell-1,2}_{n,i}), & i = 1, \ldots, P_{\ell-1}, \\ v^{\ell}_{n+1,i} = \Psi^{N_\ell}_n(\hat{v}^{\ell}_{n,i}), & i = 1, \ldots, P_{\ell}, \\ C^{\ell-1,1}_{n+1} = \overline{\mathrm{Cov}}[v^{\ell-1,1}_{n+1,1:P_{\ell-1}}], \\ C^{\ell-1,2}_{n+1} = \overline{\mathrm{Cov}}[v^{\ell-1,2}_{n+1,1:P_{\ell-1}}], \\ C^{\ell}_{n+1} = \overline{\mathrm{Cov}}[v^{\ell}_{n+1,1:P_{\ell}}], \end{cases}$$

$$\overline{\mathrm{Cov}}[v^{\ell}_{n,1:P_\ell}] := \sum_{i=1}^{P_\ell} \frac{(v^{\ell}_{n,i})(v^{\ell}_{n,i})^{\mathbf{T}}}{P_\ell} - \left(\sum_{i=1}^{P_\ell} \frac{v^{\ell}_{n,i}}{P_\ell}\right)\left(\sum_{i=1}^{P_\ell} \frac{v^{\ell}_{n,i}}{P_\ell}\right)^{\mathbf{T}},$$

$$\overline{\mathrm{Cov}}[v^{\ell-1,k}_{n,1:P_{\ell-1}}] := \sum_{i=1}^{P_{\ell-1}} \frac{(v^{\ell-1,k}_{n,i})(v^{\ell-1,k}_{n,i})^{\mathbf{T}}}{P_{\ell-1}} - \left(\sum_{i=1}^{P_{\ell-1}} \frac{v^{\ell-1,k}_{n,i}}{P_{\ell-1}}\right)\left(\sum_{i=1}^{P_{\ell-1}} \frac{v^{\ell-1,k}_{n,i}}{P_{\ell-1}}\right)^{\mathbf{T}}, \quad k=1,2.$$

(5)

$$\textbf{Update} \begin{cases} \tilde{y}^{\ell}_{n+1,i} = y_{n+1} + \eta^{\ell}_{n+1,i}, & i=1,\dots,P_\ell, \\ K^{\ell-1,1}_{n+1} = C^{\ell-1,1}_{n+1} H^{\mathbf{T}} (H C^{\ell-1,1}_{n+1} H^{\mathbf{T}} + \Gamma)^{-1}, & \\ K^{\ell-1,2}_{n+1} = C^{\ell-1,2}_{n+1} H^{\mathbf{T}} (H C^{\ell-1,2}_{n+1} H^{\mathbf{T}} + \Gamma)^{-1}, & \\ K^{\ell}_{n+1} = C^{\ell}_{n+1} H^{\mathbf{T}} (H C^{\ell}_{n+1} H^{\mathbf{T}} + \Gamma)^{-1}, & \\ \hat{v}^{\ell-1,1}_{n+1,i} = (I - K^{\ell-1,1}_{n+1} H) v^{\ell-1,1}_{n+1,i} + K^{\ell-1,1}_{n+1} \tilde{y}^{\ell}_{n+1,i}, & i=1,\dots,P_{\ell-1}, \\ \hat{v}^{\ell-1,2}_{n+1,i} = (I - K^{\ell-1,2}_{n+1} H) v^{\ell-1,2}_{n+1,i} + K^{\ell-1,2}_{n+1} \tilde{y}^{\ell}_{n+1,P_{\ell-1}+i}, & i=1,\dots,P_{\ell-1}, \\ \hat{v}^{\ell}_{n+1,i} = (I - K^{\ell}_{n+1} H) v^{\ell}_{n+1,i} + K^{\ell}_{n+1} \tilde{y}^{\ell}_{n+1,i}, & i=1,\dots,P_\ell, \end{cases}$$

where $\{\eta^{\ell}_{n+1,i}\}_{i=1}^{P_\ell}$ is a sequence of independent $N(0,\Gamma)$-distributed random variables. In the above notation, the coupling between the fine-level EnKF estimator

$$\mu^{N_\ell,P_\ell}_n[\varphi] := \sum_{i=1}^{P_\ell} \frac{\varphi(\hat{v}^{\ell}_{n,i})}{P_\ell},$$

and the two coarse-level estimators

$$\mu^{N_{\ell-1},P_{\ell-1},k}_n[\varphi] := \sum_{i=1}^{P_{\ell-1}} \frac{\varphi(\hat{v}^{\ell-1,k}_{n,i})}{P_{\ell-1}}, \qquad k=1,2$$

is obtained through particle-wise coupling

$$\hat{v}^{\ell}_{n,i} \xleftrightarrow{\text{coupling}} \begin{cases} \hat{v}^{\ell-1,1}_{n,i} & \text{if} \quad i \in \{1,\dots,P_{\ell-1}\}, \\ \hat{v}^{\ell-1,2}_{n,i-P_{\ell-1}} & \text{if} \quad i \in \{P_{\ell-1}+1,\dots,P_\ell\}. \end{cases}$$

Finally, the updated MLEnKF estimator at time n assumes the following form:

$$\mu^{ML}_n[\varphi] = \sum_{\ell=0}^{L} \sum_{m=1}^{M_\ell} \frac{\left(\mu^{N_\ell,P_\ell,m}_n - (\mu^{N_{\ell-1},P_{\ell-1},1,m}_n + \mu^{N_{\ell-1},P_{\ell-1},2,m}_n)/2\right)[\varphi]}{M_\ell} \tag{6}$$

where $\{M_\ell\}_{\ell=0}^{L} \subset \mathbb{N}$ is a decreasing sequence with M_ℓ representing the number of i.i.d. and pairwise coupled EnKF estimators on level ℓ:

$$\left\{\mu^{N_\ell,P_\ell,m}_n[\varphi], (\mu^{N_{\ell-1},P_{\ell-1},1,m}_n[\varphi], \mu^{N_{\ell-1},P_{\ell-1},2,m}_n[\varphi])\right\}_{m=1}^{M_\ell},$$

where $\mu^{N_{-1},P_{-1},m}_n[\varphi] := 0$. For the configuration of L and M_ℓ, we refer the reader to [35, Corollary 2].

3. MIEnKF

In this section, we develop the MIEnKF method by extending the MLEnKF method from the previous section.

To define a set of discretization levels for the MIEnKF, we first introduce the 2-index $\boldsymbol{\ell} := (\ell_1, \ell_2) \in \mathbb{N}_0^2$ with the shorthands $\boldsymbol{e}_1 := (1,0)$, $\boldsymbol{e}_2 := (0,1)$, and $\mathbf{1} := (1,1)$. Similarly as for MLEnKF, we associate sequences of natural numbers $N_{\ell_1} = N_0 \times 2^{\ell_1}$ and $P_{\ell_2} = P_0 \times 2^{\ell_2}$ with $N_0, P_0 \in \mathbb{N}$ to the number of timesteps and particles on the 2-index "level" $\boldsymbol{\ell}$.

Seeking to approximate $\bar{\mu}_n[\varphi]$ (the expectation of the QoI φ with respect to the mean-field measure $\bar{\mu}_n$), we denote the discrete approximation corresponding to the 2-index $\boldsymbol{\ell}$ by $\mu_n^{\boldsymbol{\ell}}[\varphi] := \mu_n^{N_{\ell_1}, P_{\ell_2}}[\varphi]$. In other words, $\mu_n^{\boldsymbol{\ell}}[\varphi]$ is the EnKF estimator (3) computed with N_{ℓ_1} timesteps and P_{ℓ_2} ensemble-members/particles. We define first-order difference operators for numbers of timesteps and particles as follows:

$$
\begin{aligned}
\Delta_1 \mu_n^{\boldsymbol{\ell}}[\varphi] &= \begin{cases} \left(\mu_n^{\boldsymbol{\ell}} - \mu_n^{\boldsymbol{\ell}-\boldsymbol{e}_1}\right)[\varphi], & \text{if } \ell_1 > 0, \\ \mu_n^{\boldsymbol{\ell}}[\varphi], & \text{if } \ell_1 = 0 \end{cases} \\
\Delta_2 \mu_n^{\boldsymbol{\ell}}[\varphi] &= \begin{cases} \left(\mu_n^{\boldsymbol{\ell}} - \left(\mu_n^{\boldsymbol{\ell}-\boldsymbol{e}_2,1} + \mu_n^{\boldsymbol{\ell}-\boldsymbol{e}_2,2}\right)/2\right)[\varphi], & \text{if } \ell_2 > 0, \\ \mu_n^{\boldsymbol{\ell}}[\varphi], & \text{if } \ell_2 = 0 \end{cases}
\end{aligned} \tag{7}
$$

where $\mu_n^{\boldsymbol{\ell}-\boldsymbol{e}_2,1}[\varphi]$ and $\mu_n^{\boldsymbol{\ell}-\boldsymbol{e}_2,2}[\varphi]$ are two i.i.d. copies of $\mu_n^{\boldsymbol{\ell}-\boldsymbol{e}_2}[\varphi]$. Note that $\mu_n^{\boldsymbol{\ell}}[\varphi]$ comprises P_{ℓ_2} ensemble members, whereas $\mu_n^{\boldsymbol{\ell}-\boldsymbol{e}_2}[\varphi]$ has half as many ensemble members, P_{ℓ_2-1}. Therefore, the pair $(\mu_n^{\boldsymbol{\ell}-\boldsymbol{e}_2,1}[\varphi], \mu_n^{\boldsymbol{\ell}-\boldsymbol{e}_2,2}[\varphi])$ are introduced to achieve a $1 \leftrightarrow 1$ coupling of ensemble-members/particles on the "levels"/2-indices $\boldsymbol{\ell}$ and $\boldsymbol{\ell} - \boldsymbol{e}_2$.

We define the four-coupled EnKF estimator using the first-order mixed difference as follows:

$$
\begin{aligned}
\boldsymbol{\Delta}\mu_n^{\boldsymbol{\ell}}[\varphi] &:= \Delta_1(\Delta_2 \mu_n^{\boldsymbol{\ell}}[\varphi]) = \Delta_2(\Delta_1 \mu_n^{\boldsymbol{\ell}}[\varphi]) = \Delta_2(\mu_n^{\boldsymbol{\ell}} - \mu_n^{\boldsymbol{\ell}-\boldsymbol{e}_1})[\varphi] \\
&= \Bigg(\mu_n^{\boldsymbol{\ell}} - \left(\mu_n^{\boldsymbol{\ell}-\boldsymbol{e}_2,1} + \mu_n^{\boldsymbol{\ell}-\boldsymbol{e}_2,2}\right)/2 \\
&\qquad - \mu_n^{\boldsymbol{\ell}-\boldsymbol{e}_1} + \left(\mu_n^{\boldsymbol{\ell}-\mathbf{1},1} + \mu_n^{\boldsymbol{\ell}-\mathbf{1},2}\right)/2 \Bigg)[\varphi],
\end{aligned} \tag{8}
$$

where the pair $(\mu_n^{\boldsymbol{\ell}-\mathbf{1},1}[\varphi], \mu_n^{\boldsymbol{\ell}-\mathbf{1},2}[\varphi])$ of i.i.d. copies of $\mu_n^{\boldsymbol{\ell}-\mathbf{1}}[\varphi]$ is also introduced to achieve a $1 \leftrightarrow 1$ coupling of ensemble-members/particles on the "levels"/2-indices $\boldsymbol{\ell}$ and $\boldsymbol{\ell} - \mathbf{1}$. If it holds that

$$
\mathbb{E}\left[\mu_n^{\boldsymbol{\ell}}[\varphi]\right] \to \bar{\mu}_n[\varphi] \quad \text{as} \quad (\ell_1, \ell_2) \to (\infty, \infty),
$$

and the sequence $\{\mathbb{E}\left[\boldsymbol{\Delta}\mu_n^{\boldsymbol{\ell}}[\varphi]\right]\}_{\boldsymbol{\ell} \in \mathbb{N}_0^2}$ is absolutely summable (both of these conditions hold under Assumption 2 (**A1**), which is presented below), then the linearity of the expectation operator implies that

$$
\bar{\mu}_n[\varphi] = \sum_{\boldsymbol{\ell} \in \mathbb{N}_0^2} \mathbb{E}\left[\boldsymbol{\Delta}\mu_n^{\boldsymbol{\ell}}[\varphi]\right] = \sum_{\boldsymbol{\ell} \in \mathcal{I}} \mathbb{E}\left[\boldsymbol{\Delta}\mu_n^{\boldsymbol{\ell}}[\varphi]\right] + \sum_{\boldsymbol{\ell} \notin \mathcal{I}} \mathbb{E}\left[\boldsymbol{\Delta}\mu_n^{\boldsymbol{\ell}}[\varphi]\right], \tag{9}
$$

for any index set $\mathcal{I} \subset \mathbb{N}_0^2$.

Remark 2. The magnitude of the second term on the right-hand side, the truncated region, relates to the bias error of the MIEnKF estimator. Accurate information on how this magnitude varies with $\mathcal{I}$ can and should be used to determine an index set such that the resulting MIEnKF method meets the bias-error constraint. In the last part of the proof of Theorem 1 below, we have indeed used Assumption 2 (**A1**) to control the bias error through bounding the magnitude of said right-hand-side term in (9).

For a given index set $\mathcal{I}$, which we will specify later in Section 4, the MIEnKF estimator is defined as the sample-average estimator of the first term on the right-hand side of (9):

$$\mu_n^{MI}[\varphi] := \sum_{\boldsymbol{\ell}\in\mathcal{I}} \sum_{m=1}^{M_{\boldsymbol{\ell}}} \frac{\boldsymbol{\Delta}\mu_n^{\boldsymbol{\ell},m}[\varphi]}{M_{\boldsymbol{\ell}}}, \tag{10}$$

where $\{\boldsymbol{\Delta}\mu_n^{\boldsymbol{\ell},m}[\varphi]\}_{m=1}^{M_{\boldsymbol{\ell}}}$ are i.i.d. copies of $\boldsymbol{\Delta}\mu_n^{\boldsymbol{\ell},m}[\varphi]$, and $\{\boldsymbol{\Delta}\mu_n^{\boldsymbol{\ell},m}[\varphi]\}_{(\boldsymbol{\ell},m)}$ are mutually independent.

The primary motivation for sampling four-coupled EnKF estimators in the MIEnKF estimator is that it leads to a substantial variance reduction that improves the tractability of the sampling method. Similar to multilevel Monte Carlo estimators, the tractability of (10) is optimized through careful selection of the index set $\mathcal{I}$ and the number of samples $M_{\boldsymbol{\ell}}$. Provided that convergence rates for the multi-index hierarchy are available or approximable, this can be achieved by solving a constrained optimization problem [29, 30].

3.1. **Four-coupled EnKF estimators.** To describe the coupling between the EnKF estimators $(\mu_n^{\boldsymbol{\ell}}, \mu_n^{\boldsymbol{\ell}-\boldsymbol{e}_2}, \mu_n^{\boldsymbol{\ell}-\boldsymbol{e}_1}, \mu_n^{\boldsymbol{\ell}-\mathbf{1}})[\varphi]$, we introduce the four-coupled updated-state ensembles at time n:

$$\{(\hat{v}_n^{\boldsymbol{\ell}}, \hat{v}_n^{\boldsymbol{\ell}-\boldsymbol{e}_2}, \hat{v}_n^{\boldsymbol{\ell}-\boldsymbol{e}_1}, \hat{v}_n^{\boldsymbol{\ell}-\mathbf{1}})_i\}_{i=1}^{P_{\ell_2}} := \{(\hat{v}_n^{\boldsymbol{\ell}}, \hat{v}_n^{\boldsymbol{\ell}-\boldsymbol{e}_2}, \hat{v}_n^{\boldsymbol{\ell}-\boldsymbol{e}_1}, \hat{v}_n^{\boldsymbol{\ell}-\mathbf{1}})(\omega_i^{\boldsymbol{\ell}})\}_{i=1}^{P_{\ell_2}}.$$

The set of particles on index $\boldsymbol{\ell}-\boldsymbol{e}_2$ is a union of two EnKF ensembles:

$$\hat{v}_{n,i}^{\boldsymbol{\ell}-\boldsymbol{e}_2,1} := \hat{v}_{n,i}^{\boldsymbol{\ell}-\boldsymbol{e}_2} \qquad i = 1, \dots P_{\ell_2-1},$$

and

$$\hat{v}_{n,i}^{\boldsymbol{\ell}-\boldsymbol{e}_2,2} := \hat{v}_{n,P_{\ell_2-1}+i}^{\boldsymbol{\ell}-\boldsymbol{e}_2} \qquad i = 1, \dots P_{\ell_2-1},$$

and the set of particles on index $\boldsymbol{\ell}-\mathbf{1}$ is also a union of two EnKF ensembles:

$$\hat{v}_{n,i}^{\boldsymbol{\ell}-\mathbf{1},1} := \hat{v}_{n,i}^{\boldsymbol{\ell}-\mathbf{1}} \qquad i = 1, \dots P_{\ell_2-1},$$

and

$$\hat{v}_{n,i}^{\boldsymbol{\ell}-\mathbf{1},2} := \hat{v}_{n,P_{\ell_2-1}+i}^{\boldsymbol{\ell}-\mathbf{1}} \qquad i = 1, \dots P_{\ell_2-1}.$$

Similarly to MLEnKF (Section 2.3), the MIEnKF employs a $1 \leftrightarrow 1$ coupling between particles on all four levels associated to one index $\boldsymbol{\ell}$. We defer further details on how this is achieved to Section 3.2, and are now ready to properly define the MIEnKF estimator.

The empirical estimator $\mu_n^{\boldsymbol{\ell}}[\varphi]$ is induced by the ensemble $\hat{v}_{n,1:P_{\ell_2}}^{\boldsymbol{\ell}} := \{\hat{v}_{n,i}^{\boldsymbol{\ell}}\}_{i=1}^{P_{\ell_2}}$, meaning that it equals the sample average of $\{\varphi(\hat{v}_{n,i}^{\boldsymbol{\ell}})\}_{i=1}^{P_{\ell_2}}$. Similarly, $\mu_n^{\boldsymbol{\ell}-\boldsymbol{e}_1}[\varphi]$ is induced by $\hat{v}_{n,1:P_{\ell_2}}^{\boldsymbol{\ell}-\boldsymbol{e}_1} := \{\hat{v}_{n,i}^{\boldsymbol{\ell}-\boldsymbol{e}_1}\}_{i=1}^{P_{\ell_2}}$,

$$\mu_n^{\boldsymbol{\ell}-\boldsymbol{e}_2}[\varphi] := \frac{(\mu_n^{\boldsymbol{\ell}-\boldsymbol{e}_2,1} + \mu_n^{\boldsymbol{\ell}-\boldsymbol{e}_2,2})[\varphi]}{2}$$

is induced by the union of two ensembles

$$\hat{v}^{\boldsymbol{\ell}-\boldsymbol{e}_2}_{n,1:P_{\ell_2}} := \{\hat{v}^{\boldsymbol{\ell}-\boldsymbol{e}_2,1}_{n,k}\}_{k=1}^{P_{\ell_2-1}} \cup \{\hat{v}^{\boldsymbol{\ell}-\boldsymbol{e}_2,2}_{n,k}\}_{k=1}^{P_{\ell_2-1}},$$

and

$$\mu_n^{\boldsymbol{\ell}-\mathbf{1}}[\varphi] := \frac{(\mu_n^{\boldsymbol{\ell}-\mathbf{1},1} + \mu_n^{\boldsymbol{\ell}-\mathbf{1},2})[\varphi]}{2}$$

is induced by $\hat{v}^{\boldsymbol{\ell}-\mathbf{1}}_{n,1:P_{\ell_2}} := \{\hat{v}^{\boldsymbol{\ell}-\mathbf{1},1}_{n,k}\}_{k=1}^{P_{\ell_2-1}} \cup \{\hat{v}^{\boldsymbol{\ell}-\mathbf{1},2}_{n,k}\}_{k=1}^{P_{\ell_2-1}}$. For consistency with (7), we impose the condition that $\mu_n^{\boldsymbol{\ell}-\boldsymbol{e}_1}[\varphi] = \mu_n^{\boldsymbol{\ell}-\mathbf{1}}[\varphi] = 0$ when $\ell_1 = 0$, and $\mu_n^{\boldsymbol{\ell}-\boldsymbol{e}_2}[\varphi] = 0$ when $\ell_2 = 0$. Figure 1 shows a visual description of all the couplings of the MIEnKF estimator.

Then, the MIEnKF estimator (10) can also be written

$$\mu_n^{MI}[\varphi] := \sum_{\boldsymbol{\ell}\in\mathcal{I}} \sum_{m=1}^{M_{\boldsymbol{\ell}}} \frac{\big(\mu_n^{\boldsymbol{\ell},m} - \mu_n^{\boldsymbol{\ell}-\boldsymbol{e}_1,m} - \mu_n^{\boldsymbol{\ell}-\boldsymbol{e}_2,m} + \mu_n^{\boldsymbol{\ell}-\mathbf{1},m}\big)[\varphi]}{M_{\boldsymbol{\ell}}} \tag{11}$$

where $\{(\mu_n^{\boldsymbol{\ell},m}, \mu_n^{\boldsymbol{\ell}-\boldsymbol{e}_1,m}, \mu_n^{\boldsymbol{\ell}-\boldsymbol{e}_2,m}, \mu_n^{\boldsymbol{\ell}-\mathbf{1},m})[\varphi]\}_m$ are independent copies of the estimators $(\mu_n^{\boldsymbol{\ell}}, \mu_n^{\boldsymbol{\ell}-\boldsymbol{e}_1}, \mu_n^{\boldsymbol{\ell}-\boldsymbol{e}_2}, \mu_n^{\boldsymbol{\ell}-\mathbf{1}})[\varphi]$ and $\{(\mu_n^{\boldsymbol{\ell},m}, \mu_n^{\boldsymbol{\ell}-\boldsymbol{e}_1,m}, \mu_n^{\boldsymbol{\ell}-\boldsymbol{e}_2,m}, \mu_n^{\boldsymbol{\ell}-\mathbf{1},m})[\varphi]\}_{(\boldsymbol{\ell},m)}$ are mutually independent.

Remark 3. For comparison, the MLEnKF estimator (6) takes the following form when represented in the above 2-index notation

$$\mu_n^{ML}[\varphi] = \sum_{\ell=0}^{L} \sum_{m=1}^{M_\ell} \frac{\big(\mu_n^{(\ell,\ell),m} - \mu_n^{(\ell,\ell)-\mathbf{1},m}\big)[\varphi]}{M_\ell}.$$

3.2. **Particle-wise four-coupling for MIEnKF.** We now describe how the four-coupling of EnKF estimators manifests itself particle by particle. At time $n = 0$, the fine-index update ensemble $\{\hat{v}^{\boldsymbol{\ell}}_{0,i}\}_{i=1}^{P_{\ell_2}}$ comprises independent $\mathbb{P}_{u_0|Y_0}$-distributed samples that are particle-wisely coupled to three other ensembles by

$$\hat{v}^{\boldsymbol{\ell}}_{0,i} = \hat{v}^{\boldsymbol{\ell}-\boldsymbol{e}_1}_{0,i} = \hat{v}^{\boldsymbol{\ell}-\boldsymbol{e}_2}_{0,i} = \hat{v}^{\boldsymbol{\ell}-\mathbf{1}}_{0,i} \qquad \text{for} \quad i = 1, 2 \ldots, P_{\ell_2}.$$

To describe how the coupling enters in the prediction-update iterations of the particles, let us consider the update state of a foursome $(\hat{v}^{\boldsymbol{\ell}}_{n,i}, \hat{v}^{\boldsymbol{\ell}-\boldsymbol{e}_1}_{n,i}, \hat{v}^{\boldsymbol{\ell}-\boldsymbol{e}_2}_{n,i}, \hat{v}^{\boldsymbol{\ell}-\mathbf{1}}_{n,i})$ at time $n \geq 0$. The next-time prediction state of the foursome is given by

$$\begin{aligned} v^{\boldsymbol{\ell}}_{n+1,i} &= \Psi_n^{N_{\ell_1}}(\hat{v}^{\boldsymbol{\ell}}_{n,i}), \qquad v^{\boldsymbol{\ell}-\boldsymbol{e}_1}_{n+1,i} = \Psi_n^{N_{\ell_1-1}}(\hat{v}^{\boldsymbol{\ell}-\boldsymbol{e}_1}_{n,i}), \\ v^{\boldsymbol{\ell}-\boldsymbol{e}_2}_{n+1,i} &= \Psi_n^{N_{\ell_1}}(\hat{v}^{\boldsymbol{\ell}-\boldsymbol{e}_2}_{n,i}), \qquad v^{\boldsymbol{\ell}-\mathbf{1}}_{n+1,i} = \Psi_n^{N_{\ell_1-1}}(\hat{v}^{\boldsymbol{\ell}-\mathbf{1}}_{n,i}), \end{aligned} \tag{12}$$

where the four particles share the same driving noise in the dynamics. The sample covariance matrices and Kalman gains are expressed as follows:

$$\begin{aligned} C^{\boldsymbol{\ell}}_{n+1} &= \overline{\mathrm{Cov}}[v^{\boldsymbol{\ell}}_{n+1}], \qquad K^{\boldsymbol{\ell}}_{n+1} = C^{\boldsymbol{\ell}}_{n+1} H^{\mathbf{T}} (H C^{\boldsymbol{\ell}}_{n+1} H^{\mathbf{T}} + \Gamma)^{-1}, \\ C^{\boldsymbol{\ell}-\boldsymbol{e}_1}_{n+1} &= \overline{\mathrm{Cov}}[v^{\boldsymbol{\ell}-\boldsymbol{e}_1}_{n+1}], \qquad K^{\boldsymbol{\ell}-\boldsymbol{e}_1}_{n+1} = C^{\boldsymbol{\ell}-\boldsymbol{e}_1}_{n+1} H^{\mathbf{T}} (H C^{\boldsymbol{\ell}-\boldsymbol{e}_1}_{n+1} H^{\mathbf{T}} + \Gamma)^{-1}, \end{aligned} \tag{13}$$

and

$$\begin{aligned} C^{\boldsymbol{\ell}-\boldsymbol{e}_2,1}_{n+1} &= \overline{\mathrm{Cov}}[v^{\boldsymbol{\ell}-\boldsymbol{e}_2,1}_{n+1}], \qquad K^{\boldsymbol{\ell}-\boldsymbol{e}_2,1}_{n+1} = C^{\boldsymbol{\ell}-\boldsymbol{e}_2,1}_{n+1} H^{\mathbf{T}} (H C^{\boldsymbol{\ell}-\boldsymbol{e}_2,1}_{n+1} H^{\mathbf{T}} + \Gamma)^{-1}, \\ C^{\boldsymbol{\ell}-\boldsymbol{e}_2,2}_{n+1} &= \overline{\mathrm{Cov}}[v^{\boldsymbol{\ell}-\boldsymbol{e}_2,2}_{n+1}], \qquad K^{\boldsymbol{\ell}-\boldsymbol{e}_2,2}_{n+1} = C^{\boldsymbol{\ell}-\boldsymbol{e}_2,2}_{n+1} H^{\mathbf{T}} (H C^{\boldsymbol{\ell}-\boldsymbol{e}_2,2}_{n+1} H^{\mathbf{T}} + \Gamma)^{-1}, \\ C^{\boldsymbol{\ell}-\mathbf{1},1}_{n+1} &= \overline{\mathrm{Cov}}[v^{\boldsymbol{\ell}-\mathbf{1},1}_{n+1}], \qquad K^{\boldsymbol{\ell}-\mathbf{1},1}_{n+1} = C^{\boldsymbol{\ell}-\mathbf{1},1}_{n+1} H^{\mathbf{T}} (H C^{\boldsymbol{\ell}-\mathbf{1},1}_{n+1} H^{\mathbf{T}} + \Gamma)^{-1}, \\ C^{\boldsymbol{\ell}-\mathbf{1},2}_{n+1} &= \overline{\mathrm{Cov}}[v^{\boldsymbol{\ell}-\mathbf{1},2}_{n+1}], \qquad K^{\boldsymbol{\ell}-\mathbf{1},2}_{n+1} = C^{\boldsymbol{\ell}-\mathbf{1},2}_{n+1} H^{\mathbf{T}} (H C^{\boldsymbol{\ell}-\mathbf{1},2}_{n+1} H^{\mathbf{T}} + \Gamma)^{-1}, \end{aligned} \tag{14}$$

where we recall that index $\boldsymbol{\ell}-\boldsymbol{e}_2$ and index $\boldsymbol{\ell}-\mathbf{1}$ both consist of two EnKF ensembles of size P_{ℓ_2-1}, cf. Section 3.1. The perturbed observations are also particle-wisely coupled, so that one obtains the updated states:

$$\left.\begin{aligned} \tilde{y}^{\boldsymbol{\ell}}_{n+1,i} &= y_{n+1} + \eta^{\boldsymbol{\ell}}_{n+1,i}, \\ \hat{v}^{\boldsymbol{\ell}}_{n+1,i} &= (I - K^{\boldsymbol{\ell}}_{n+1}H)v^{\boldsymbol{\ell}}_{n+1,i} + K^{\boldsymbol{\ell}}_{n+1}\tilde{y}^{\boldsymbol{\ell}}_{n+1,i}, \\ \hat{v}^{\boldsymbol{\ell}-\boldsymbol{e}_1}_{n+1,i} &= (I - K^{\boldsymbol{\ell}-\boldsymbol{e}_1}_{n+1}H)v^{\boldsymbol{\ell}-\boldsymbol{e}_1}_{n+1,i} + K^{\boldsymbol{\ell}-\boldsymbol{e}_1}_{n+1}\tilde{y}^{\boldsymbol{\ell}}_{n+1,i}, \end{aligned}\right\} \quad i = 1, \dots, P_{\ell_2}\,, \tag{15}$$

and

$$\left.\begin{aligned} \hat{v}^{\boldsymbol{\ell}-\boldsymbol{e}_2,1}_{n+1,i} &= (I - K^{\boldsymbol{\ell}-\boldsymbol{e}_2,1}_{n+1}H)v^{\boldsymbol{\ell}-\boldsymbol{e}_2,1}_{n+1,i} + K^{\boldsymbol{\ell}-\boldsymbol{e}_2,1}_{n+1}\tilde{y}^{\boldsymbol{\ell}}_{n+1,i}, \\ \hat{v}^{\boldsymbol{\ell}-\boldsymbol{e}_2,2}_{n+1,i} &= (I - K^{\boldsymbol{\ell}-\boldsymbol{e}_2,2}_{n+1}H)v^{\boldsymbol{\ell}-\boldsymbol{e}_2,2}_{n+1,i} + K^{\boldsymbol{\ell}-\boldsymbol{e}_2,2}_{n+1}\tilde{y}^{\boldsymbol{\ell}}_{n+1,i+P_{\ell_2-1}}, \\ \hat{v}^{\boldsymbol{\ell}-\mathbf{1},1}_{n+1,i} &= (I - K^{\boldsymbol{\ell}-\mathbf{1},1}_{n+1}H)v^{\boldsymbol{\ell}-\mathbf{1},1}_{n+1,i} + K^{\boldsymbol{\ell}-\mathbf{1},1}_{n+1}\tilde{y}^{\boldsymbol{\ell}}_{n+1,i}, \\ \hat{v}^{\boldsymbol{\ell}-\mathbf{1},2}_{n+1,i} &= (I - K^{\boldsymbol{\ell}-\mathbf{1},2}_{n+1}H)v^{\boldsymbol{\ell}-\mathbf{1},2}_{n+1,i} + K^{\boldsymbol{\ell}-\mathbf{1},2}_{n+1}\tilde{y}^{\boldsymbol{\ell}}_{n+1,i+P_{\ell_2-1}}, \end{aligned}\right\} \quad i = 1, \dots, P_{\ell_2-1}\,, \tag{16}$$

where $\{\eta^{\ell_2}_{n+1,i}\}_{i=1}^{P_{\ell_2}}$ are i.i.d. with $\eta^{\ell_2}_{n+1,1} \sim N(0,\Gamma)$.

To summarize, four ensembles are particle-wisely coupled by sharing the initial condition, the driving noise, and perturbed observations. A sketch of one prediction-update iteration of the MIEnKF method and the composition of the MIEnKF estimator is provided in Figure 1 and Algorithm 1 describes the essential steps of the MIEnKF method.

4. MIEnKF complexity

This section presents a cost-versus-accuracy result for the MIEnKF method, and compares the performance of MIEnKF to MLEnKF and EnKF.

Let us first recall that we restrict ourselves to resolutions of the form

$$N_{\ell_1} = N_0 \times 2^{\ell_1} \quad \text{and} \quad P_{\ell_2} = P_0 \times 2^{\ell_2} \qquad \forall \boldsymbol{\ell} \in \mathbb{N}_0^2,$$

for some $N_0, P_0 \in \mathbb{N}$, and proceed with defining the notion of admissible QoIs:

Definition 1 (Admissible QoI)**.** A Borel-measurable mapping $\varphi : \mathbb{R}^d \to \mathbb{R}$ is said to be an admissible QoI if it satisfies the following two integrability conditions for all $n \geq 0$:

$$\bar{\mu}_n[\varphi] < \infty \quad \text{and} \quad \mu^{\boldsymbol{\ell}}_n[\varphi] \in L^2(\Omega) \quad \forall \boldsymbol{\ell} \in \mathbb{N}_0^2.$$

For any admissible QoI and $\boldsymbol{\ell} \in \mathbb{N}_0^2$, the definition implies that $\boldsymbol{\Delta}\mu^{\boldsymbol{\ell}}_n[\varphi] \in L^2(\Omega)$, and we impose the additional assumptions to ensure good performance for MIEnKF:

Assumption 2. For any admissible QoI φ and any $n \geq 0$, the four-coupled EnKF estimator $\boldsymbol{\Delta}\mu^{\boldsymbol{\ell}}_n[\varphi]$ satisfies the following conditions:

$$\left|\mathbb{E}\left[\boldsymbol{\Delta}\mu^{\boldsymbol{\ell}}_n[\varphi]\right]\right| \lesssim N_{\ell_1}^{-1} P_{\ell_2}^{-1}, \tag{A1}$$

$$\mathbb{V}[\boldsymbol{\Delta}\mu^{\boldsymbol{\ell}}_n[\varphi]] \lesssim N_{\ell_1}^{-2} P_{\ell_2}^{-2}, \tag{A2}$$

and

$$\mathrm{Cost}(\boldsymbol{\Delta}\mu^{\boldsymbol{\ell}}_n[\varphi]) \eqsim N_{\ell_1} P_{\ell_2}. \tag{A3}$$

[2]

[2]The constraint (A3) could be stated as a property rather than an assumption, as it holds by construction. Every prediction-update iteration of the coupled EnKF ensembles relating to $\boldsymbol{\Delta}\mu^{\boldsymbol{\ell}}_n$ costs $\mathcal{O}(N_{\ell_1} P_{\ell_2})$, cf. Section 3.2.

Algorithm 1: MIEnKF

Input: The model parameters, the QoI φ, the final time $\mathcal{N}$, the observation operator H, observations $\{y_n\}_{n=1}^{\mathcal{N}}$, m_0, Σ_0, Γ, L, $M_{\boldsymbol{\ell}}$, N_{ℓ_1}, P_{ℓ_2}.

Output: The MIEnKF estimator $\mu_n^{MI}[\varphi]$.

for $\boldsymbol{\ell} \in \mathcal{I}$ **do**
  for $m = 1 : M_{\boldsymbol{\ell}}$ **do**
    Initialize the ensembles at time $n = 0$ by sampling $\hat{v}_{0,i}^{\boldsymbol{\ell},m} \sim N(m_0, \Sigma_0)$ and setting $\hat{v}_{0,i}^{\boldsymbol{\ell},m} = \hat{v}_{0,i}^{\boldsymbol{\ell}-\boldsymbol{e}_1,m} = \hat{v}_{0,i}^{\boldsymbol{\ell}-\boldsymbol{e}_2,m} = \hat{v}_{0,i}^{\boldsymbol{\ell}-\mathbf{1},m}$ for $i = 1, ..., P_{\ell_2}$.
for $n = 1 : \mathcal{N}$ **do**
  for $\boldsymbol{\ell} \in \mathcal{I}$ **do**
    for $m = 1 : M_{\boldsymbol{\ell}}$ **do**
      if $\ell_1 = 0$ *and* $\ell_2 = 0$ **then**
        Compute the EnKF prediction states for $i = 1, ..., P_{\ell_2}$ $v_{n,i}^{\boldsymbol{\ell},m} = \textbf{Prediction}(\hat{v}_{n-1,i}^{\boldsymbol{\ell},m})$ similar to (1).
        Compute the EnKF updated states for $i = 1, ..., P_{\ell_2}$ $\hat{v}_{n,i}^{\boldsymbol{\ell},m} = \textbf{Update}(v_{n,i}^{\boldsymbol{\ell},m})$ similar to (2).
        Compute the EnKF estimator $\boldsymbol{\Delta}\mu_n^{\boldsymbol{\ell},m}[\varphi] = \sum_{i=1}^{P_{\ell_2}} \frac{\varphi(\hat{v}_{n,i}^{\boldsymbol{\ell},m})}{P_{\ell_2}}$.
      else if $\ell_1 > 0$ *and* $\ell_2 = 0$ **then**
        Compute pairwise coupled prediction states for $i = 1, ..., P_{\ell_2}$ $v_{n,i}^{\boldsymbol{\ell},m}, v_{n,i}^{\boldsymbol{\ell}-\boldsymbol{e}_1,m} = \textbf{Prediction}(\hat{v}_{n-1,i}^{\boldsymbol{\ell},m}, \hat{v}_{n-1,i}^{\boldsymbol{\ell}-\boldsymbol{e}_1,m})$ similar to (4).
        Compute pairwise coupled updated states for $i = 1, ..., P_{\ell_2}$ $\hat{v}_{n,i}^{\boldsymbol{\ell},m}, \hat{v}_{n,i}^{\boldsymbol{\ell}-\boldsymbol{e}_1,m} = \textbf{Update}(v_{n,i}^{\boldsymbol{\ell},m}, v_{n,i}^{\boldsymbol{\ell}-\boldsymbol{e}_1,m})$ similar to (5).
        Compute the EnKF estimator pairwise coupled in N_{ℓ_1} $\boldsymbol{\Delta}\mu_n^{\boldsymbol{\ell},m}[\varphi] = \sum_{i=1}^{P_{\ell_2}} \frac{\varphi(\hat{v}_{n,i}^{\boldsymbol{\ell},m}) - \varphi(\hat{v}_{n,i}^{\boldsymbol{\ell}-\boldsymbol{e}_1,m})}{P_{\ell_2}}$.
      else if $\ell_1 = 0$ *and* $\ell_2 > 0$ **then**
        Compute pairwise coupled prediction states for $i = 1, ..., P_{\ell_2}$ $v_{n,i}^{\boldsymbol{\ell},m}, v_{n,i}^{\boldsymbol{\ell}-\boldsymbol{e}_2,m} = \textbf{Prediction}(\hat{v}_{n-1,i}^{\boldsymbol{\ell},m}, \hat{v}_{n-1,i}^{\boldsymbol{\ell}-\boldsymbol{e}_2,m})$ similar to (12)-(14).
        Compute pairwise coupled updated states for $i = 1, ..., P_{\ell_2}$ $\hat{v}_{n,i}^{\boldsymbol{\ell},m}, \hat{v}_{n,i}^{\boldsymbol{\ell}-\boldsymbol{e}_2,m} = \textbf{Update}(v_{n,i}^{\boldsymbol{\ell},m}, v_{n,i}^{\boldsymbol{\ell}-\boldsymbol{e}_2,m})$ similar to (15)- (16).
        Compute the EnKF estimator pairwise coupled in P_{ℓ_2} $\boldsymbol{\Delta}\mu_n^{\boldsymbol{\ell},m}[\varphi] = \sum_{i=1}^{P_{\ell_2}} \frac{\varphi(\hat{v}_{n,i}^{\boldsymbol{\ell},m}) - \varphi(\hat{v}_{n,i}^{\boldsymbol{\ell}-\boldsymbol{e}_2,m})}{P_{\ell_2}}$.
      else if $\ell_1 > 0$ *and* $\ell_2 > 0$ **then**
        Compute the four-coupled prediction states for $i = 1, ..., P_{\ell_2}$ $v_{n,i}^{\boldsymbol{\ell},m}, v_{n,i}^{\boldsymbol{\ell}-\boldsymbol{e}_1,m}, v_{n,i}^{\boldsymbol{\ell}-\boldsymbol{e}_2,m}, \hat{v}_{n,i}^{\boldsymbol{\ell}-\mathbf{1},m} = \textbf{Prediction}(\hat{v}_{n-1,i}^{\boldsymbol{\ell},m}, \hat{v}_{n-1,i}^{\boldsymbol{\ell}-\boldsymbol{e}_1,m}, \hat{v}_{n-1,i}^{\boldsymbol{\ell}-\boldsymbol{e}_2,m}, \hat{v}_{n-1,i}^{\boldsymbol{\ell}-\mathbf{1},m})$ by (12)-(14).
        Compute the four-coupled updated states for $i = 1, ..., P_{\ell_2}$ $\hat{v}_{n,i}^{\boldsymbol{\ell},m}, \hat{v}_{n,i}^{\boldsymbol{\ell}-\boldsymbol{e}_1,m}, \hat{v}_{n,i}^{\boldsymbol{\ell}-\boldsymbol{e}_2,m}, \hat{v}_{n,i}^{\boldsymbol{\ell}-\mathbf{1},m} = \textbf{Update}(v_{n,i}^{\boldsymbol{\ell},m}, v_{n,i}^{\boldsymbol{\ell}-\boldsymbol{e}_1,m}, v_{n,i}^{\boldsymbol{\ell}-\boldsymbol{e}_2,m}, \hat{v}_{n,i}^{\boldsymbol{\ell}-\mathbf{1},m})$ by (15)-(16).
        Compute the four-coupled EnKF estimator $\boldsymbol{\Delta}\mu_n^{\boldsymbol{\ell},m}[\varphi] = \sum_{i=1}^{P_{\ell_2}} \frac{\varphi(\hat{v}_{n,i}^{\boldsymbol{\ell},m}) - \varphi(\hat{v}_{n,i}^{\boldsymbol{\ell}-\boldsymbol{e}_1,m}) - \varphi(\hat{v}_{n,i}^{\boldsymbol{\ell}-\boldsymbol{e}_2,m}) + \varphi(\hat{v}_{n,i}^{\boldsymbol{\ell}-\mathbf{1},m})}{P_{\ell_2}}$.
  Compute the MIEnKF estimator $\mu_n^{MI}[\varphi] = \sum_{\boldsymbol{\ell}\in\mathcal{I}} \sum_{m=1}^{M_{\boldsymbol{\ell}}} \frac{\boldsymbol{\Delta}\mu_n^{\boldsymbol{\ell},m}[\varphi]}{M_{\boldsymbol{\ell}}}$.

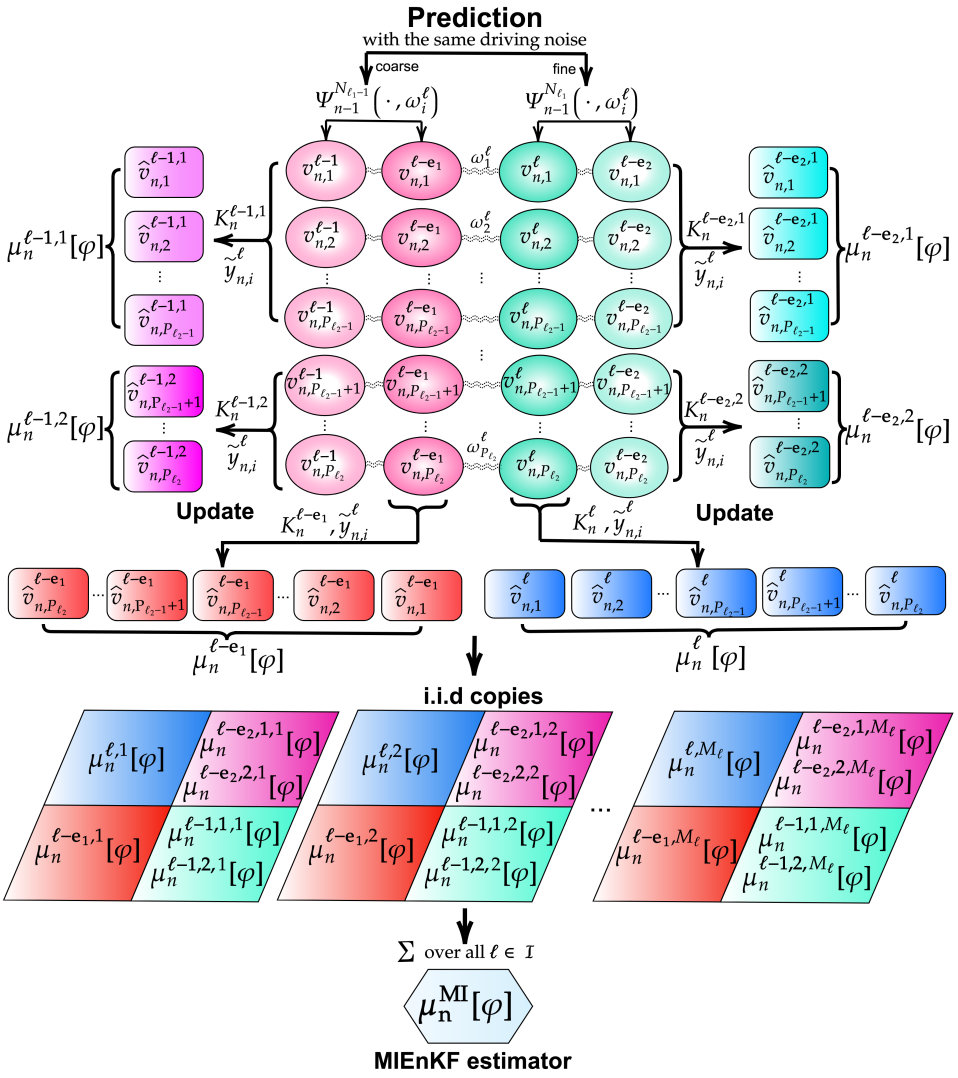


FIGURE 1. One prediction-update iteration of the multi-index ensemble Kalman filtering (MIEnKF) estimator described in Section 3.2. The ovals represent four-coupled prediction-state particles, sharing the same driving noise $\omega^{\boldsymbol{\ell}}$ and coupled initial conditions. The respective squares represent updated-state particles sharing the same perturbed observations.

Theorem 1 (MIEnKF complexity)**.** *Let Assumptions 1 and 2 hold, and for any* $\epsilon > 0$ *consider the MIEnKF method with triangular index set* $\mathcal{I} = \{\boldsymbol{\ell} \in \mathbb{N}_0^2 \mid \ell_1 + \ell_2 \leq L\}$*, where*

$$L = \max\left(\lceil \log \epsilon^{-1} + \log\log \epsilon^{-1} \rceil - L_0,\ 1\right) \quad \textit{for some} \quad L_0 \in \mathbb{N}_0$$

and the number of samples

$$M_{\boldsymbol{\ell}} \eqsim \epsilon^{-2} N_{\ell_1}^{-3/2} P_{\ell_2}^{-3/2} \qquad \boldsymbol{\ell} \in \mathcal{I}.$$

For any admissible QoI φ and $n \geq 0$, it then holds that

$$\mathbb{E}\left[\left(\mu_n^{MI}[\varphi] - \bar{\mu}_n[\varphi]\right)^2\right] \lesssim \epsilon^2, \tag{17}$$

and the computational cost of the MIEnKF estimator satisfies that

$$\mathrm{Cost}(\mu_{\mathrm{n}}^{\mathrm{MI}}[\varphi]) \eqsim \epsilon^{-2}.$$

Proof. Adding and subtracting $\mathbb{E}\left[\mu_n^{MI}[\varphi]\right]$ in the mean-squared error, we obtain

$$\mathbb{E}\left[\left(\mu_n^{MI}[\varphi] \pm \mathbb{E}\left[\mu_n^{MI}[\varphi]\right] - \bar{\mu}_n[\varphi]\right)^2\right] = \mathbb{V}\left[\mu_n^{MI}[\varphi]\right] + \left(\mathbb{E}\left[\mu_n^{MI}[\varphi]\right] - \bar{\mu}_n[\varphi]\right)^2.$$

For the variance term, the independence of the random variables $\{\boldsymbol{\Delta}\mu_n^{\boldsymbol{\ell},m}[\varphi]\}_{(\boldsymbol{\ell},m)}$ and (**A2**) yield

$$\mathbb{V}\left[\mu_n^{MI}[\varphi]\right] = \sum_{\boldsymbol{\ell}\in\mathcal{I}} \sum_{m=1}^{M_{\boldsymbol{\ell}}} \frac{\mathbb{V}\left[\boldsymbol{\Delta}\mu_n^{\boldsymbol{\ell},m}[\varphi]\right]}{M_{\boldsymbol{\ell}}} \lesssim \sum_{\boldsymbol{\ell}\in\mathcal{I}} M_{\boldsymbol{\ell}}^{-1} N_{\ell_1}^{-2} P_{\ell_2}^{-2} \lesssim \epsilon^2.$$

For the squared bias term, (**A1**) and the multi-index telescoping properties of the MIEnKF estimator imply that

$$\left(\mathbb{E}\left[\mu_n^{MI}[\varphi]\right] - \bar{\mu}_n[\varphi]\right)^2 \leq \left(\sum_{\boldsymbol{\ell}\notin\mathcal{I}} \mathbb{E}\left[\boldsymbol{\Delta}\mu_n^{\boldsymbol{\ell}}[\varphi]\right]\right)^2 \lesssim \left(\sum_{\boldsymbol{\ell}\notin\mathcal{I}} N_{\ell_1}^{-1} P_{\ell_2}^{-1}\right)^2.$$

The mean-squared error bound (17) follows by

$$\sum_{\boldsymbol{\ell}\notin\mathcal{I}} N_{\ell_1}^{-1} P_{\ell_2}^{-1} \lesssim \sum_{\ell_1+\ell_2>L}^{\infty} 2^{-(\ell_1+\ell_2)} = \sum_{k=L+1}^{\infty} (k+1)2^{-k} \eqsim 2^{-L} L \eqsim \epsilon$$

and

$$\mathrm{Cost}(\mu_n^{MI}[\varphi]) = \sum_{\boldsymbol{\ell}\in\mathcal{I}} M_{\boldsymbol{\ell}} \mathrm{Cost}(\boldsymbol{\Delta}\mu_n^{\boldsymbol{\ell}}[\varphi]) \eqsim \sum_{\boldsymbol{\ell}\in\mathcal{I}} M_{\boldsymbol{\ell}} N_{\ell_1} P_{\ell_2} \eqsim \epsilon^{-2}.$$ [3]

□

Remark 4. For comparison, we briefly recall the cost-versus-accuracy results for EnKF and MLEnKF. For any $\epsilon > 0$ and sufficient regularity

$$\left\|(\mu_n^{N,P} - \bar{\mu}_n)[\varphi]\right\|_p \lesssim \epsilon, \qquad \text{(EnKF)}$$
$$\left\|(\mu_n^{ML} - \bar{\mu}_n)[\varphi]\right\|_p \lesssim \epsilon, \qquad \text{(MLEnKF)}$$

with the computational cost bounded by

$$\mathrm{Cost}(\mu_n^{N,P}[\varphi]) \eqsim \epsilon^{-3},$$
$$\mathrm{Cost}(\mu_n^{ML}[\varphi]) \eqsim \epsilon^{-2} \left|\log(\epsilon)\right|^3.$$

For more details, see [35].

Remark 5. An alternative to (**A2**) that is more aligned with assumption made for the existing convergence results for MLEnKF is to assume that

$$\left\|\boldsymbol{\Delta}\mu_n^{\boldsymbol{\ell}}[\varphi]\right\|_p \lesssim N_{\ell_1}^{-1} P_{\ell_2}^{-1}, \tag{**A2***}$$

[3] Optimal choices for L and $M_{\boldsymbol{\ell}}$ in Theorem 1 can be obtained by solving a constrained optimization problem, analogously as elaborated on for the MLMC method in the seminal paper [24].

for $p \geq 2$. Then, using the same aforementioned index set $\mathcal{I}$ and L and with a slight change in the sample size $M_{\boldsymbol{\ell}} \eqsim \epsilon^{-2} N_{\ell_1}^{-4/3} P_{\ell_2}^{-4/3}$, the MIEnKF estimator satisfies

$$\left\| (\mu_n^{MI} - \bar{\mu}_n)[\varphi] \right\|_p \lesssim \epsilon, \tag{18}$$

with the asymptotic MIEnKF cost bounded by $\mathcal{O}(\epsilon^{-2})$. This can be proved similarly as the case of Theorem 1, where the L_p-norm of the statistical error can be bounded using the Marcinkiewicz-Zygmund inequality:

$$\begin{aligned} \left\| (\mu_n^{MI} - \bar{\mu}_n)[\varphi] \right\|_p &\leq \left\| \mu_n^{MI}[\varphi] - \mathbb{E}[\mu_n^{MI}][\varphi] \right\|_p + \left\| \mathbb{E}[\mu_n^{MI}][\varphi] - \bar{\mu}_n[\varphi] \right\|_p \\ &\lesssim \sum_{\boldsymbol{\ell} \in \mathcal{I}} M_{\boldsymbol{\ell}}^{-1/2} \left\| \boldsymbol{\Delta} \mu_n^{\boldsymbol{\ell},m}[\varphi] \right\|_p + \sum_{\boldsymbol{\ell} \notin \mathcal{I}} \left| \mathbb{E}[\boldsymbol{\Delta} \mu_n^{\boldsymbol{\ell},m}[\varphi]] \right|. \end{aligned}$$

We note that (**A2**) is a weaker assumption than (**A2***) since

$$\mathbb{V}\left[\boldsymbol{\Delta} \mu_n^{\boldsymbol{\ell}}[\varphi] \right] \leq \left\| \boldsymbol{\Delta} \mu_n^{\boldsymbol{\ell}}[\varphi] \right\|_2^2 \leq \left\| \boldsymbol{\Delta} \mu_n^{\boldsymbol{\ell}}[\varphi] \right\|_p^2. \tag{19}$$

Remark 6. Under more general settings, Assumption 2 may be transformed into

$$\left| \mathbb{E}[\boldsymbol{\Delta} \mu_n^{\boldsymbol{\ell}}[\varphi]] \right| \lesssim N_{\ell_1}^{-\alpha_1} P_{\ell_2}^{-\alpha_2}, \tag{$\mathcal{A}_1$}$$

$$\left\| \boldsymbol{\Delta} \mu_n^{\boldsymbol{\ell}}[\varphi] \right\|_p \lesssim N_{\ell_1}^{-\beta_1} P_{\ell_2}^{-\beta_2}, \tag{$\mathcal{A}_2$}$$

$$\mathrm{Cost}(\boldsymbol{\Delta} \mu_n^{\boldsymbol{\ell}}[\varphi]) \eqsim N_{\ell_1}^{\gamma_1} P_{\ell_2}^{\gamma_2}, \tag{$\mathcal{A}_3$}$$

for some $\alpha_1, \alpha_2, \beta_1, \beta_2, \gamma_1, \gamma_2 > 0$. The construction of an efficient MIEnKF estimator may then lead to a differently shaped (possibly even non-triangular) index set $\mathcal{I}$, a different sequence of number of samples $\{M_{\boldsymbol{\ell}}\}_{\boldsymbol{\ell} \in \mathcal{I}}$, and other common ratios for the geometric sequences $\{N_{\ell_1}\}$ and $\{P_{\ell_2}\}$. The problem of optimizing the set $\mathcal{I}$ may be recast as a knapsack problem, which is a well-studied optimization problem with many available solution algorithms, cf. [29] and [30, equation (21)]. For instance, the approach developed for approximations of multi-index Monte Carlo applied to McKean-Vlasov dynamics in [30] defines the set by

$$\mathcal{I} = \{(\ell_1, \ell_2) \in \mathbb{N}_0^2 : (\alpha_1 + \gamma_1)\ell_1 + (\alpha_2 + \gamma_2)\ell_2 \leq L\}.$$

5. Numerical examples

This section presents a numerical comparison of MIEnKF with the EnKF and MLEnKF methods outlined in Section 2. Three problems will be considered: the Ornstein-Uhlenbeck (OU) process, a stochastic differential equation (SDE) with a double-well (DW) potential, and Langevin dynamics [34, 35, 6, 4, 18].

We consider SDE on the general form

$$du = -U'(u)dt + \sigma dW_t, \tag{20}$$

with a constant diffusion coefficient $\sigma = 0.5$ and two types of potential functions:

(i) $U(u) = u^2/2$, **(OU)**
(ii) $U(u) = u^2/4 + 1/(4u^2 + 2)$, **(DW)**.

The numerical discretizations of (20) are computed using the Milstein numerical scheme[4] with uniform timestep $\Delta t = 1/N$ for any $N \geq 1$. The observations of

[4]Note that in all three examples considered, the SDEs are with constant diffusion terms. For such SDEs, the Milstein scheme coincides with the Euler-Maruyama scheme.

the process u are equally spaced with observation time interval $\tau = 1$, observation operator $H = 1$, $\Gamma = 0.1$ and the QoI $\varphi(x) = x$.

To numerically verify assumptions (**A1**) and (**A2***), the following rates are estimated from S independent copies of $\boldsymbol{\Delta}\mu_n^{\boldsymbol{\ell}}[\varphi]$:

$$\left|\mathbb{E}[\boldsymbol{\Delta}\mu_n^{\boldsymbol{\ell}}[\varphi]]\right| \approx \Big|\sum_{i=1}^{S} \frac{\boldsymbol{\Delta}\mu_{n,i}^{\boldsymbol{\ell}}[\varphi]}{S}\Big|,$$

$$\left\|\boldsymbol{\Delta}\mu_n^{\boldsymbol{\ell}}[\varphi]\right\|_2 \approx \sqrt{\frac{1}{S}\sum_{i=1}^{S}\left|\boldsymbol{\Delta}\mu_{n,i}^{\boldsymbol{\ell}}[\varphi]\right|^2}.$$

We analyze the convergence rates of the methods by computing the time-averaged root-mean-squared error (RMSE).

$$\text{RMSE} := \sqrt{\frac{1}{S(\mathcal{N}+1)}\sum_{i=1}^{S}\sum_{n=0}^{\mathcal{N}}\left|\mu_{n,i}^{*}[\varphi] - \bar{\mu}_n[\varphi]\right|^2},$$

where $\{\mu_{\cdot,i}^{*}[\varphi]\}_{i=1}^{S}$ are independent copies of $\mu_{\cdot}^{*}[\varphi]$ for the specific methods (EnKF, MLEnKF, and MIEnKF).

5.1. **Reference solutions and computer architecture.** Since dynamics Ψ is linear for the OU problem, the reference solution $\bar{\mu}_n[\varphi]$ can be computed exactly using the Kalman filter. However, the reference solution for the DW problem, which involves nonlinear dynamics, must be approximated. This solution is computed using the deterministic mean-field EnKF algorithm, cf. [35, Appendix C]. A pseudoreference solution for the final test problem based on Langevin dynamics is computed by the sample average of $S = 180$ independent simulations of the MIEnKF estimator at the tolerance $\epsilon = 2^{-11}$ using the following parameters:

$$\begin{aligned}
L &= \lceil L_* + \log_2(L_*)\rceil - 1, \qquad \text{with} \quad L_* = \lceil \log_2(\epsilon^{-1})\rceil - 1,\\
N_{\ell_1} &= 4 \times 2^{\ell_1},\\
P_{\ell_2} &= 30 \times 2^{\ell_2},\\
M_{\boldsymbol{\ell}} &= \begin{cases} 6 \times \lceil \epsilon^{-2} N_{\ell_1}^{-3/2} P_{\ell_2}^{-3/2}\rceil & \text{if} \quad \ell_1 = 0 \text{ and } \ell_2 = 0,\\ 90 \times \lceil \epsilon^{-2} N_{\ell_1}^{-3/2} P_{\ell_2}^{-3/2}\rceil & \text{if} \quad 1 \le \ell_1 + \ell_2 \le L. \end{cases}
\end{aligned}$$

The numerical simulations were computed in parallel on 18 cores on an Intel(R) Xeon(R) CPU E5-2680 v2 20-core processor with 128 GB RAM. The computer code was written in the Julia programming language [14], and it can be downloaded from https://github.com/GaukharSH/mienkf.

5.2. **Ornstein-Uhlenbeck process.** We consider the SDE (20) with the (OU) potential function and initial condition $u(0) \sim N(0, \Gamma)$. Convergence rates (**A1**) and (**A2***) shown in Figure 2 were estimated by the Monte Carlo method using $S = 10^6$ independent samples of $\boldsymbol{\Delta}\mu_n^{\boldsymbol{\ell}}[\varphi]$. In the figure, the left panel shows the weak and L_2 convergence rates over $\mathcal{N} = 10$ observation times with $(\ell_1 + \ell_2) \in [0, 7]$, and the right panel shows the ratio of the rates to $N_{\ell_1}^{-1} P_{\ell_2}^{-1}$. The plane-like flatness of the right panel for $(\ell_1 + \ell_2) \in [1, 7]$ validates the said rate assumptions.

When conducting runtime-versus-accuracy convergence tests for an input tolerance $\epsilon > 0$, we set the parameters of the respective methods as follows:

$$\textbf{EnKF:} \quad P = \lceil 15\epsilon^{-2} \rceil \quad \text{and} \quad N = \lceil \epsilon^{-1} \rceil, \tag{21}$$

$$\textbf{MLEnKF:} \quad \begin{cases} L = \lceil \log_2(\epsilon^{-1}) \rceil - 1, \\ N_\ell = 2 \times 2^\ell, \\ P_\ell = 10 \times 2^\ell, \\ M_\ell = \begin{cases} 2 \times \lceil \epsilon^{-2} L^2 2^{-3} \rceil & \text{if} \quad \ell = 0, \\ \lceil \epsilon^{-2} L^2 2^{-2\ell-3} \rceil & \text{if} \quad 1 \le \ell \le L, \end{cases} \end{cases} \tag{22}$$

and

$$\textbf{MIEnKF:} \quad \begin{cases} L = \lceil L_* + \log_2(L_*) \rceil - 1, \quad \text{with} \quad L_* = \lceil \log_2(\epsilon^{-1}) \rceil - 1, \\ N_{\ell_1} = 4 \times 2^{\ell_1}, \\ P_{\ell_2} = 30 \times 2^{\ell_2}, \\ M_{\boldsymbol{\ell}} = \begin{cases} 6 \times \lceil \epsilon^{-2} N_{\ell_1}^{-3/2} P_{\ell_2}^{-3/2} \rceil & \text{if} \quad \ell_1 = 0 \text{ and } \ell_2 = 0, \\ 120 \times \lceil \epsilon^{-2} N_{\ell_1}^{-3/2} P_{\ell_2}^{-3/2} \rceil & \text{if} \quad 1 \le \ell_1 + \ell_2 \le L. \end{cases} \end{cases} \tag{23}$$

For a sequence of predefined tolerances $\epsilon = [2^{-4}, 2^{-5}, 2^{-6}, 2^{-7}, 2^{-8}, 2^{-9}]$ for EnKF and MLEnKF, and $\epsilon = [2^{-4}, 2^{-5}, 2^{-6}, 2^{-7}, 2^{-8}, 2^{-9}, 2^{-10}, 2^{-11}]$ for MIEnKF, Figure 3 shows the runtime against the RMSE for the three methods over observation times of $\mathcal{N} = 10$ and $\mathcal{N} = 100$ estimated using $S = 100$ independent runs. MIEnKF outperforms EnKF and MLEnKF for sufficiently small tolerances, and the complexity rate agrees with the theory.

5.3. **Double-well SDE.** We consider the SDE (20) with the DW potential function and $u(0) \sim N(0, \Gamma)$. Similar to the OU case, Figure 4 provides numerical evidence of the conjecture rates under assumptions (**A1**) and (**A2***). For the same predefined $\epsilon-$inputs with the same degrees of freedom setting as in the example of OU, the performance of the three methods were compared in terms of runtime against RMSE for observation times $\mathcal{N} = 10$ and $\mathcal{N} = 100$ and estimated over $S = 100$ independent runs (Figure 5). We observe that MIEnKF outperforms EnKF and MLEnKF for small RMSE.

5.4. **Langevin SDE.** In the last example, we consider the two-dimensional stochastic Langevin dynamics

$$\begin{aligned} dX_t &= V_t dt, \\ dV_t &= -U'(X_t)dt - \kappa V_t dt + (2\kappa T)^{1/2} dW_t, \end{aligned} \tag{24}$$

where X_t and V_t denotes the particle position and velocity, respectively, $U(X)$ is the previously introduced DW potential, $\kappa = 2^{-5} \times \pi^2$ is the viscosity and $T = 1$ is the temperature. To improve the pairwise coupling between particles, we used the first-order symplectic Euler splitting scheme [52]. The initial conditions are provided by $X_0 \sim N(0, \Gamma)$ and $V_0 \sim N(0, \Gamma)$ with X_0 and V_0 being independent. Further, based on initial test runs, the method parameters are set to

$$\textbf{EnKF:} \quad P = \lceil 10\epsilon^{-2} \rceil \quad \text{and} \quad N = \lceil \epsilon^{-1} \rceil,$$

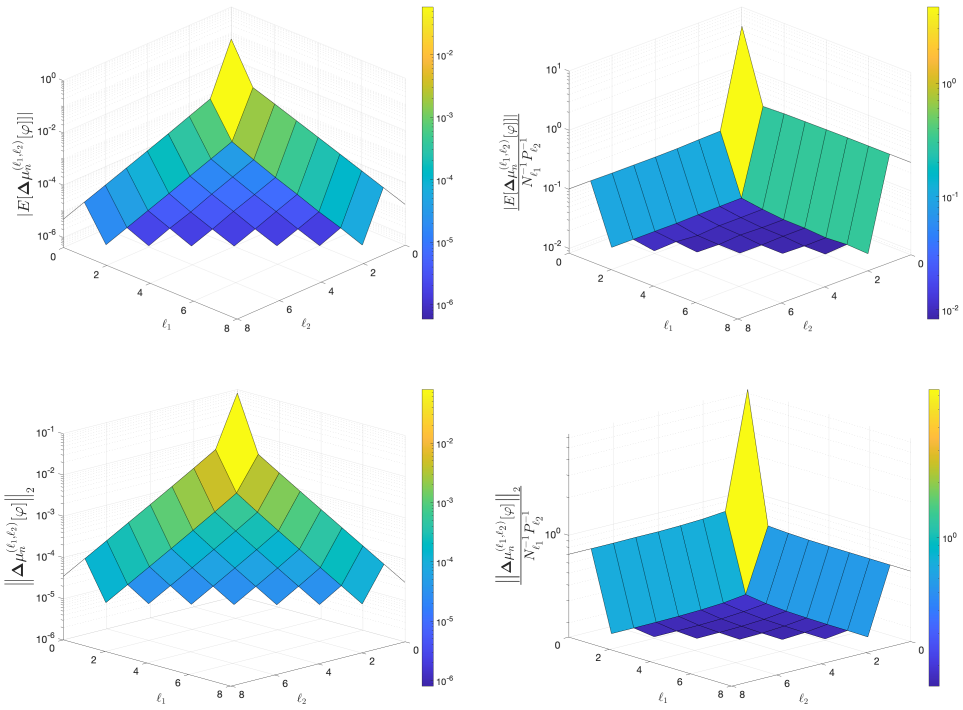


FIGURE 2. **Ornstein-Uhlenbeck problem. Estimates based on $S = 10^6$ independent runs (Section 5.2).** Top row: Numerical evidence of assumption (A1) over $\mathcal{N} = 20$ observation times when using $N_{\ell_1} = 4 \times 2^{\ell_1}$ and $P_{\ell_2} = 20 \times 2^{\ell_2}$. Bottom row: Similar plots for the verification of assumption (A2*).

$$\textbf{MLEnKF:} \quad \begin{cases} L = \lceil \log_2(\epsilon^{-1}) \rceil - 1, \\ N_\ell = 2 \times 2^\ell, \\ P_\ell = 8 \times 2^\ell, \\ M_\ell = \begin{cases} 2 \times \lceil \epsilon^{-2} L^2 2^{-2} \rceil & \text{if} \quad \ell = 0, \\ \lceil \epsilon^{-2} L^2 2^{-2\ell-2} \rceil & \text{if} \quad 1 \le \ell \le L, \end{cases} \end{cases}$$

and

$$\textbf{MIEnKF:} \quad \begin{cases} L = \lceil L_* + \log_2(L_*) \rceil - 1, \quad \text{with} \quad L_* = \lceil \log_2(\epsilon^{-1}) \rceil - 1 \\ N_{\ell_1} = 4 \times 2^{\ell_1}, \\ P_{\ell_2} = 20 \times 2^{\ell_2}, \\ M_{\boldsymbol{\ell}} = \begin{cases} 6 \times \lceil \epsilon^{-2} N_{\ell_1}^{-3/2} P_{\ell_2}^{-3/2} \rceil & \text{if} \quad \ell_1 = 0 \text{ and } \ell_2 = 0, \\ 50 \times \lceil \epsilon^{-2} N_{\ell_1}^{-3/2} P_{\ell_2}^{-3/2} \rceil & \text{if} \quad 1 \le \ell_1 + \ell_2 \le L. \end{cases} \end{cases}$$

To shed some light on the importance of the temperature parameter, Figure 6 illustrates the phase-portrait time evolution of the realization of Langevin dynamics up to the final time $\mathcal{N} = 50$ for different temperatures $T = [0,\ 0.01,\ 0.1,\ 1.0]$. Damping causes a rapid decay of the velocity from the initial value to zero when

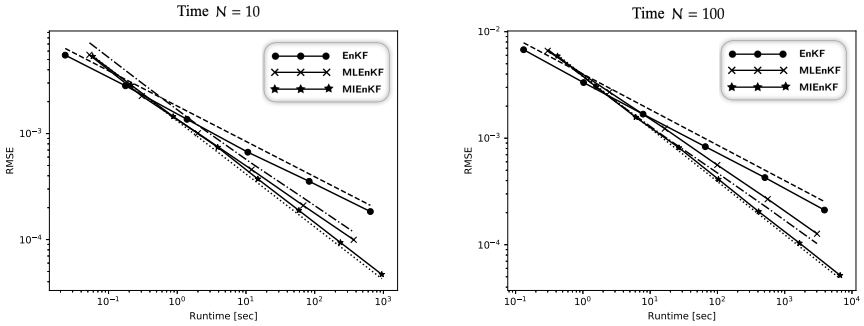


FIGURE 3. **Ornstein-Uhlenbeck problem. Estimates based on $S = 100$ independent runs (Section 5.2).** Comparison of the runtime versus root-mean-squared error (RMSE) for mean over observation times $\mathcal{N} = 10$ (left) and $\mathcal{N} = 100$ (right). The solid-crossed line represents MLEnKF and the dot-dashed line is a fitted $\mathcal{O}(\log(10+\text{Runtime})^{1/3}\text{Runtime}^{-1/2})$ reference line. The solid-asterisk line represents the MIEnKF and the dotted line is a fitted $\mathcal{O}(\text{Runtime}^{-1/2})$ reference line. The solid-bulleted line represents EnKF and the dashed line is a fitted $\mathcal{O}(\text{Runtime}^{-1/3})$ reference line.

$T = 0$. For positive temperatures, thermal fluctuation leads to more diffusive dynamics. Figure 7 shows the signal-tracking performance of MIEnKF for the full observation operator

$$H = \begin{bmatrix} 1 & 0 \\ 0 & 1 \end{bmatrix}$$

and the partial observation operators $H = [1\ 0]$ or $H = [0\ 1]$, all computed at the tolerance $\epsilon = 2^{-7}$. The method is tracking the true state of the observed components well in all cases, but, as is to be expected, it does not track the true state of unobserved components with the same level of accuracy. The numerical verification of assumptions (**A1**) and (**A2***) with respect to different observation operators is shown in Figures 8 and 9, respectively. For a sequence of predefined tolerances, $\epsilon = [2^{-4}, 2^{-5}, \ldots, 2^{-9}]$ for EnKF and MLEnKF and $\epsilon = [2^{-4}, 2^{-5}, \ldots, 2^{-10}]$ for MIEnKF, we compare the performance of the three methods in terms of runtime versus RMSE. We consider $\mathcal{N} = 10$ and $\mathcal{N} = 20$ observation times, the QoI $\varphi(X, V) = X$ and $\varphi(X, V) = V$, and we use $S = 90$ independent runs of each method to estimate both RMSE and runtime. Figures 10 and 11 show the results for the observation operators

$$H = [1\ 0] \quad \text{and} \quad H = \begin{bmatrix} 1 & 0 \\ 0 & 1 \end{bmatrix},$$

respectively. The observed complexity rates for MIEnKF are close to the theory, and the method is more efficient than the alternatives for small tolerances in both cases.

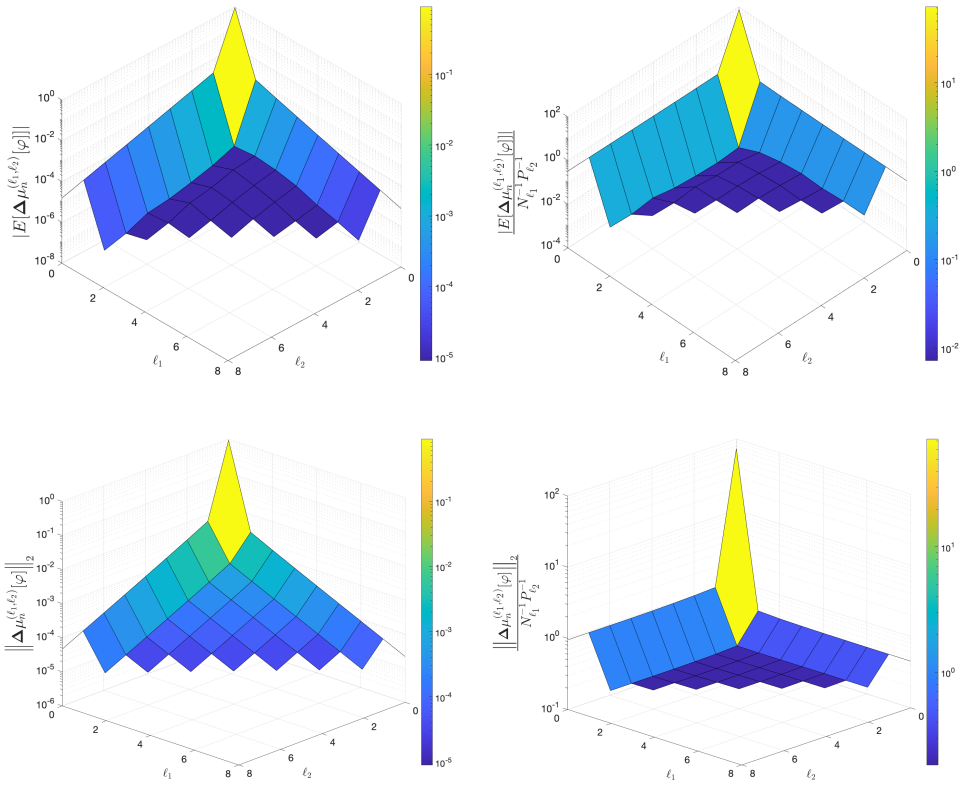


FIGURE 4. **Double Well problem. Estimates based on $S = 10^6$ independent runs (Section 5.3).** Top row: Numerical evidence of assumption (**A1**) for $\mathcal{N} = 10$ observation times when using $N_{\ell_1} = 4\times 2^{\ell_1}$ and $P_{\ell_2} = 20\times 2^{\ell_2}$. Bottom row: Similar plots for verifying assumption (**A2***).

6. Conclusion

We have developed a hierarchical ensemble-based filtering method called the MIEnKF method. MIEnKF is based on independent samples of four-coupled EnKF estimators on a multi-index hierarchy of resolution levels. Under Assumptions 1 and 2, we proved that the method is highly efficient and that it will asymptotically outperform the comparable methods EnKF and MLEnKF. For instance, when the weak convergence rate $\alpha = 1$ and the strong convergence rate $\beta = 2$, which is a more robust setting of the EnKF and MLEnKF methods considered in [35], the computational cost of reaching $\mathcal{O}(\epsilon^2)$ MSE is $\mathcal{O}(\epsilon^{-2})$ for MIEnKF, $\mathcal{O}(\epsilon^{-2}|\log(\epsilon)|^3)$ for MLEnKF, and $\mathcal{O}(\epsilon^{-3})$ for EnKF.

In this work we have constructed a multi-index EnKF method with two resolution parameters: N_{ℓ_1} relating to the time-discretization, and the ensemble-size P_{ℓ_2}, a 2-index MIEnKF method. For more complicated high-dimensional filtering problems, it is an open question if it is possible to extend MIEnKF to having more resolution parameters, and whether that would lead to further performance

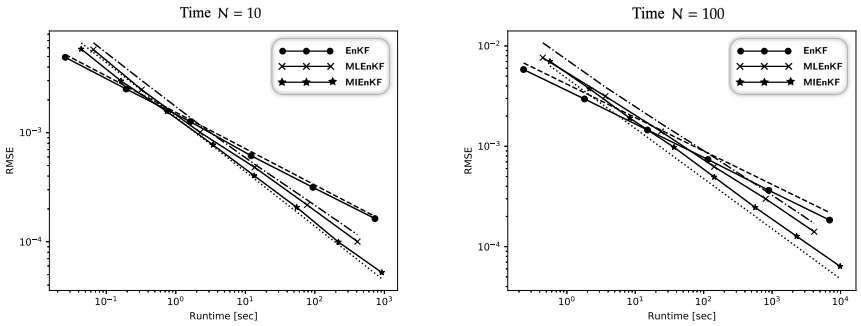


FIGURE 5. **Double Well problem. Estimates based on $S = 100$ independent runs (Section 5.3).** Similar plots as those shown in Figure 3.

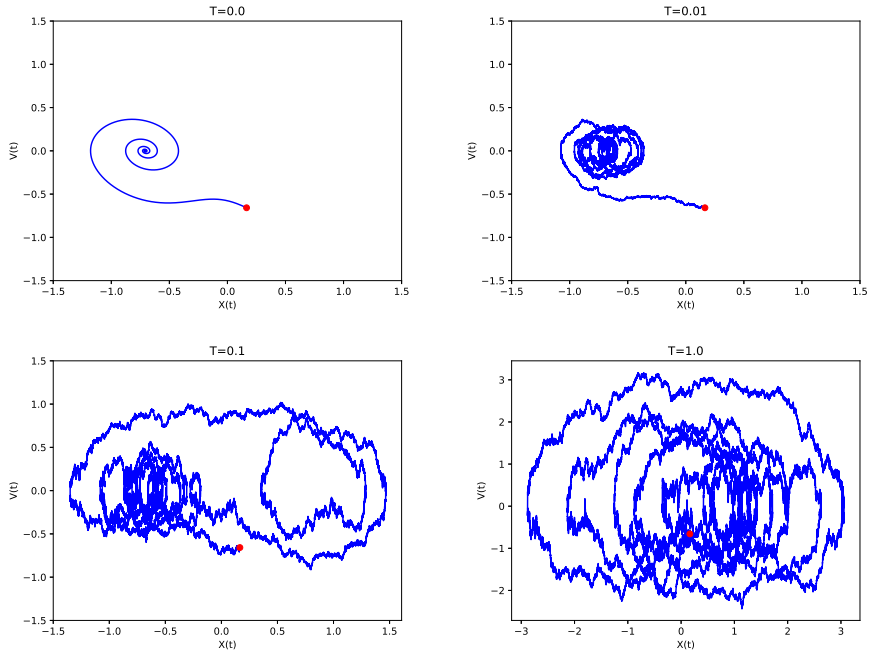


FIGURE 6. **Time evolution of a solution to Langevin dynamics with different temperature T values**. The symplectic Euler scheme is used up to final time $\mathcal{N} = 50$. The red dot represents the initial value.

gains. One extension we currently working on is a 3-index MIEnKF for spatiotemporal models that are discretized in both space and time, e.g., reaction-diffusion stochastic partial differential equations (SPDE) [17].

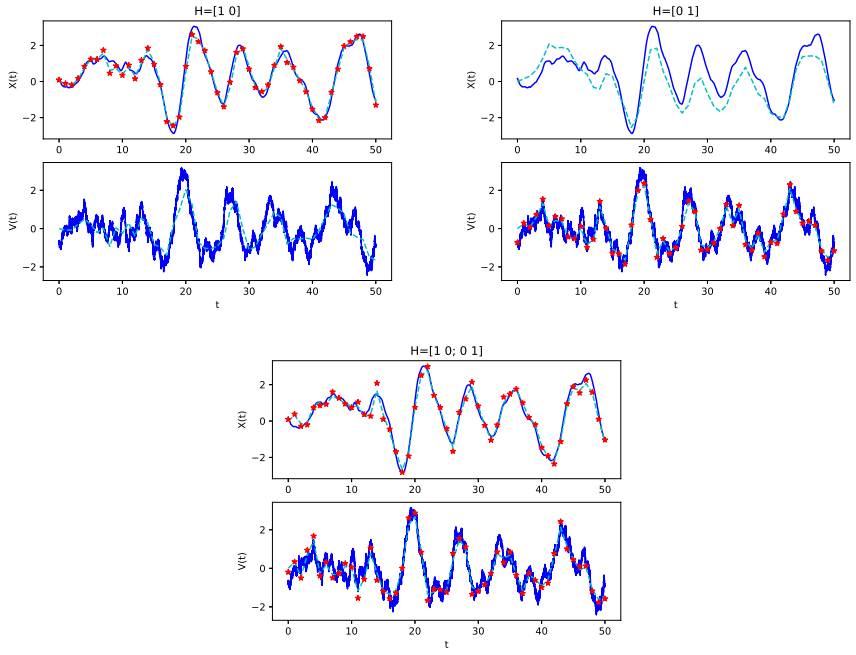


FIGURE 7. **Data assimilation for Langevin dynamics given different observation operators H, Section 5.4.** The blue solid line represents the truth, and the red stars are the observations. The cyan dashed lines represent MIEnKF mean. The final time $\mathcal{N} = 50$ is used with the observation timestep $\tau = 1.0$

Another interesting direction would be MIEnKF for filtering problems with high-frequency or continuous-time observations. Here, the new challenge is that low-resolution levels have to be updated – has to assimilate observations – at a lower frequency than high-resolution levels, but strong coupling still has to be preserved. The recent work on MLEnKF for Kalman-Bucy filters [16] would be a good starting point for developing an MIEnKF method for such problem settings.

Acknowledgments This work was supported by the KAUST Office of Sponsored Research (OSR) under Award No. URF/1/2584-01-01 and the Alexander von Humboldt Foundation. G. Shaimerdenova and R. Tempone are members of the KAUST SRI Center for Uncertainty Quantification in Computational Science and Engineering.

REFERENCES

[1] Sigurd I Aanonsen, Geir Nævdal, Dean S Oliver, Albert C Reynolds, Brice Vallès, et al. The ensemble Kalman filter in reservoir engineering–a review. *Spe Journal*, 14(03):393–412, 2009.

[2] Mohamed Ben Alaya, Ahmed Kebaier, and Thi Bao Tram Ngo. Central Limit Theorem for the σ-antithetic multilevel Monte Carlo method. *arXiv preprint arXiv:2002.08834*, 2020.

[3] Jeffrey L Anderson. An ensemble adjustment Kalman filter for data assimilation. *Monthly weather review*, 129(12):2884–2903, 2001.

[4] Amit Apte, Martin Hairer, AM Stuart, and Jochen Voss. Sampling the posterior: An approach to non-Gaussian data assimilation. *Physica D: Nonlinear Phenomena*, 230(1-2):50–64, 2007.

[5] Jayesh Badwaik, Christian Klingenberg, Nils Henrik Risebro, and Adrian M Ruf. Multilevel monte carlo finite volume methods for random conservation laws with discontinuous flux. *ESAIM: Mathematical Modelling and Numerical Analysis*, 55(3):1039–1065, 2021.

[6] Marco Ballesio, Ajay Jasra, Erik von Schwerin, and Raul Tempone. A Wasserstein coupled particle filter for multilevel estimation. *arXiv preprint arXiv:2004.03981*, 2020.

[7] Theo Baracchini, Philip Y Chu, Jonas Šukys, Gian Lieberherr, Stefan Wunderle, Alfred Wüest, and Damien Bouffard. Data assimilation of in situ and satellite remote sensing data to 3d hydrodynamic lake models: a case study using delft3d-flow v4. 03 and openda v2. 4. *Geoscientific Model Development*, 13(3):1267–1284, 2020.

[8] Andrea Barth and Andreas Stein. A study of elliptic partial differential equations with jump diffusion coefficients. *SIAM/ASA Journal on Uncertainty Quantification*, 6(4):1707–1743, 2018.

[9] Andrea Beck, Jakob Dürrwächter, Thomas Kuhn, Fabian Meyer, Claus-Dieter Munz, and Christian Rohde. hp-multilevel Monte Carlo methods for uncertainty quantification of compressible Navier–Stokes equations. *SIAM Journal on Scientific Computing*, 42(4):B1067–B1091, 2020.

[10] Joakim Beck, Ben Mansour Dia, Luis Espath, and Raúl Tempone. Multilevel double loop Monte Carlo and stochastic collocation methods with importance sampling for Bayesian optimal experimental design. *International Journal for Numerical Methods in Engineering*, 121(15):3482–3503, 2020.

[11] Thomas Bengtsson, Peter Bickel, and Bo Li. Curse-of-dimensionality revisited: Collapse of the particle filter in very large scale systems. In *Probability and statistics: Essays in honor of David A. Freedman*, pages 316–334. Institute of Mathematical Statistics, 2008.

[12] Alexandros Beskos, Ajay Jasra, Kody Law, Youssef Marzouk, and Yan Zhou. Multilevel sequential Monte Carlo with dimension-independent likelihood-informed proposals. *SIAM/ASA Journal on Uncertainty Quantification*, 6(2):762–786, 2018.

[13] Alexandros Beskos, Ajay Jasra, Kody Law, Raul Tempone, and Yan Zhou. Multilevel sequential Monte Carlo samplers. *Stochastic Processes and their Applications*, 127(5):1417–1440, 2017.

[14] Jeff Bezanson, Alan Edelman, Stefan Karpinski, and Viral B Shah. Julia: A fresh approach to numerical computing. *SIAM Review*, 59(1):65–98, 2017.

[15] Craig H Bishop, Brian J Etherton, and Sharanya J Majumdar. Adaptive sampling with the ensemble transform Kalman filter. part i: Theoretical aspects. *Monthly weather review*, 129(3):420–436, 2001.

[16] Neil K Chada, Ajay Jasra, and Fangyuan Yu. Multilevel ensemble Kalman-Bucy filters. *arXiv preprint arXiv:2011.04342*, 2020.

[17] Alexey Chernov, Håkon Hoel, Kody JH Law, Fabio Nobile, and Raul Tempone. Multilevel ensemble Kalman filtering for spatio-temporal processes. *Numerische Mathematik*, pages 1–55, 2020.

[18] Hugh L Christensen, James Murphy, and Simon J Godsill. Forecasting high-frequency futures returns using online langevin dynamics. *IEEE Journal of Selected Topics in Signal Processing*, 6(4):366–380, 2012.

[19] Gianluca Detommaso, Tim Dodwell, and Rob Scheichl. Continuous level Monte Carlo and sample-adaptive model hierarchies. *SIAM/ASA Journal on Uncertainty Quantification*, 7(1):93–116, 2019.

[20] Geir Evensen. Sequential data assimilation with a nonlinear quasi-geostrophic model using Monte Carlo methods to forecast error statistics. *Journal of Geophysical Research: Oceans*, 99(C5):10143–10162, 1994.

[21] Wei Fang and Mike B Giles. Importance sampling for pathwise sensitivity of stochastic chaotic systems. *SIAM/ASA Journal on Uncertainty Quantification*, 9(3):1217–1241, 2021.

[22] Kristian Fossum, Trond Mannseth, and Andreas S Stordal. Assessment of multilevel ensemble-based data assimilation for reservoir history matching. *Computational Geosciences*, 24(1):217–239, 2020.

[23] Han Gao and Jian-Xun Wang. A bi-fidelity ensemble kalman method for pde-constrained inverse problems in computational mechanics. *Computational Mechanics*, 67(4):1115–1131, 2021.

[24] Michael B Giles. Multilevel monte carlo path simulation. *Operations research*, 56(3):607–617, 2008.

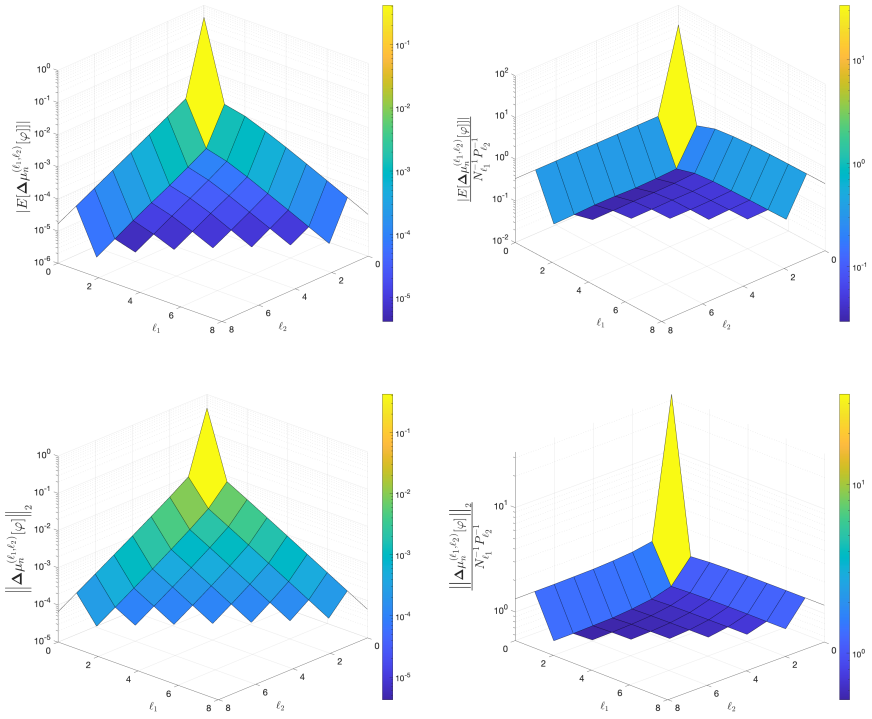
[25] Michael B Giles and Benjamin J Waterhouse. Multilevel quasi-Monte Carlo path simulation. *Advanced Financial Modelling, Radon Series on Computational and Applied Mathematics*, 8:165–181, 2009.
[26] Takashi Goda, Tomohiko Hironaka, and Takeru Iwamoto. Multilevel Monte Carlo estimation of expected information gains. *Stochastic Analysis and Applications*, 38(4):581–600, 2020.
[27] Alastair Gregory and Colin J Cotter. A seamless multilevel ensemble transform particle filter. *SIAM Journal on Scientific Computing*, 39(6):A2684–A2701, 2017.
[28] Alastair Gregory, Colin J Cotter, and Sebastian Reich. Multilevel ensemble transform particle filtering. *SIAM Journal on Scientific Computing*, 38(3):A1317–A1338, 2016.
[29] Abdul-Lateef Haji-Ali, Fabio Nobile, and Raúl Tempone. Multi-index Monte Carlo: when sparsity meets sampling. *Numerische Mathematik*, 132(4):767–806, 2016.
[30] Abdul-Lateef Haji-Ali and Raúl Tempone. Multilevel and multi-index Monte Carlo methods for the Mckean–Vlasov equation. *Statistics and Computing*, 28(4):923–935, 2018.
[31] Mohamad Abed El Rahman Hammoud, Issam Lakkis, Omar Knio, and Ibrahim Hoteit. Moving source identification in an uncertain marine flow: Mediterranean Sea application. *Ocean Engineering*, 220:108435, 2021.
[32] Chiheb Ben Hammouda, Nadhir Ben Rached, and Raúl Tempone. Importance sampling for a robust and efficient multilevel Monte Carlo estimator for stochastic reaction networks. *Statistics and Computing*, 30(6):1665–1689, 2020.
[33] Håkon Hoel and Sebastian Krumscheid. Central limit theorems for multilevel Monte Carlo methods. *Journal of Complexity*, 54:101407, 2019.
[34] Håkon Hoel, Kody JH Law, and Raúl Tempone. Multilevel ensemble Kalman filtering. *SIAM Journal on Numerical Analysis*, 54(3):1813–1839, 2016.
[35] Håkon Hoel, Gaukhar Shaimerdenova, and Raúl Tempone. Multilevel ensemble Kalman filtering based on a sample average of independent enkf estimators. *Foundations of Data Science*, 2(4):351, 2020.
[36] Peter L Houtekamer and Herschel L Mitchell. Data assimilation using an ensemble Kalman filter technique. *Monthly Weather Review*, 126(3):796–811, 1998.
[37] Peter L Houtekamer, Herschel L Mitchell, Gérard Pellerin, Mark Buehner, Martin Charron, Lubos Spacek, and Bjarne Hansen. Atmospheric data assimilation with an ensemble Kalman filter: Results with real observations. *Monthly weather review*, 133(3):604–620, 2005.
[38] Ajay Jasra, Kengo Kamatani, Kody JH Law, and Yan Zhou. Multilevel particle filters. *SIAM Journal on Numerical Analysis*, 55(6):3068–3096, 2017.
[39] Benjamin Jourdain, Ahmed Kebaier, et al. Non-asymptotic error bounds for the multilevel Monte Carlo euler method applied to sdes with constant diffusion coefficient. *Electronic Journal of Probability*, 24, 2019.
[40] Eugenia Kalnay. *Atmospheric modeling, data assimilation and predictability*. Cambridge university press, 2003.
[41] Ahmed Kebaier and Jérôme Lelong. Coupling importance sampling and multilevel Monte Carlo using sample average approximation. *Methodology and Computing in Applied Probability*, 20(2):611–641, 2018.
[42] Amirreza Khodadadian, Maryam Parvizi, and Clemens Heitzinger. An adaptive multilevel Monte Carlo algorithm for the stochastic drift–diffusion–poisson system. *Computer Methods in Applied Mechanics and Engineering*, 368:113163, 2020.
[43] Frances Kuo, Robert Scheichl, Christoph Schwab, Ian Sloan, and Elisabeth Ullmann. Multilevel quasi-Monte Carlo methods for lognormal diffusion problems. *Mathematics of Computation*, 86(308):2827–2860, 2017.
[44] Jonas Latz, Iason Papaioannou, and Elisabeth Ullmann. Multilevel sequential2 Monte Carlo for Bayesian inverse problems. *Journal of Computational Physics*, 368:154–178, 2018.
[45] Kody JH Law, Hamidou Tembine, and Raul Tempone. Deterministic mean-field ensemble kalman filtering. *SIAM Journal on Scientific Computing*, 38(3):A1251–A1279, 2016.
[46] François Le Gland, Valérie Monbet, and Vu-Duc Tran. *Large sample asymptotics for the ensemble Kalman filter*. PhD thesis, INRIA, 2009.
[47] Alexander Litvinenko, Abdulkadir C Yucel, Hakan Bagci, Jesper Oppelstrup, Eric Michielssen, and Raúl Tempone. Computation of electromagnetic fields scattered from objects with uncertain shapes using multilevel Monte Carlo method. *IEEE Journal on Multiscale and Multiphysics Computational Techniques*, 4:37–50, 2019.

[48] Kjetil O Lye, Siddhartha Mishra, and Roberto Molinaro. A multi-level procedure for enhancing accuracy of machine learning algorithms. *European Journal of Applied Mathematics*, 32(3):436–469, 2021.
[49] Jan Mandel, Loren Cobb, and Jonathan D Beezley. On the convergence of the ensemble Kalman filter. *Applications of Mathematics*, 56(6):533–541, 2011.
[50] Gabriel Moldovan, Guillame Lehnasch, Laurent Cordier, and Marcello Meldi. A multigrid/ensemble kalman filter strategy for assimilation of unsteady flows. *Journal of Computational Physics*, 443:110481, 2021.
[51] Pierre Del Moral, Ajay Jasra, Kody JH Law, and Yan Zhou. Multilevel sequential Monte Carlo samplers for normalizing constants. *ACM Transactions on Modeling and Computer Simulation (TOMACS)*, 27(3):1–22, 2017.
[52] Eike H Müller, Rob Scheichl, and Tony Shardlow. Improving multilevel Monte Carlo for stochastic differential equations with application to the Langevin equation. *Proceedings of the Royal Society A: Mathematical, Physical and Engineering Sciences*, 471(2176):20140679, 2015.
[53] Andrey A Popov, Changhong Mou, Adrian Sandu, and Traian Iliescu. A multifidelity ensemble kalman filter with reduced order control variates. *SIAM Journal on Scientific Computing*, 43(2):A1134–A1162, 2021.
[54] Andrey A Popov and Adrian Sandu. Multifidelity ensemble Kalman filtering using surrogate models defined by physics-informed autoencoders. *arXiv preprint arXiv:2102.13025*, 2021.
[55] Pieterjan Robbe, Dirk Nuyens, and Stefan Vandewalle. Recycling samples in the multigrid multilevel (quasi-) Monte Carlo method. *SIAM Journal on Scientific Computing*, 41(5):S37–S60, 2019.
[56] Sangeetika Ruchi, Svetlana Dubinkina, and Jana de Wiljes. Fast hybrid tempered ensemble transform filter formulation for Bayesian elliptical problems via Sinkhorn approximation. *Nonlinear Processes in Geophysics*, 28(1):23–41, 2021.
[57] Daniel Schaden and Elisabeth Ullmann. On multilevel best linear unbiased estimators. *SIAM/ASA Journal on Uncertainty Quantification*, 8(2):601–635, 2020.
[58] Søren Taverniers and Daniel M Tartakovsky. Estimation of distributions via multilevel Monte Carlo with stratified sampling. *Journal of Computational Physics*, 419:109572, 2020.

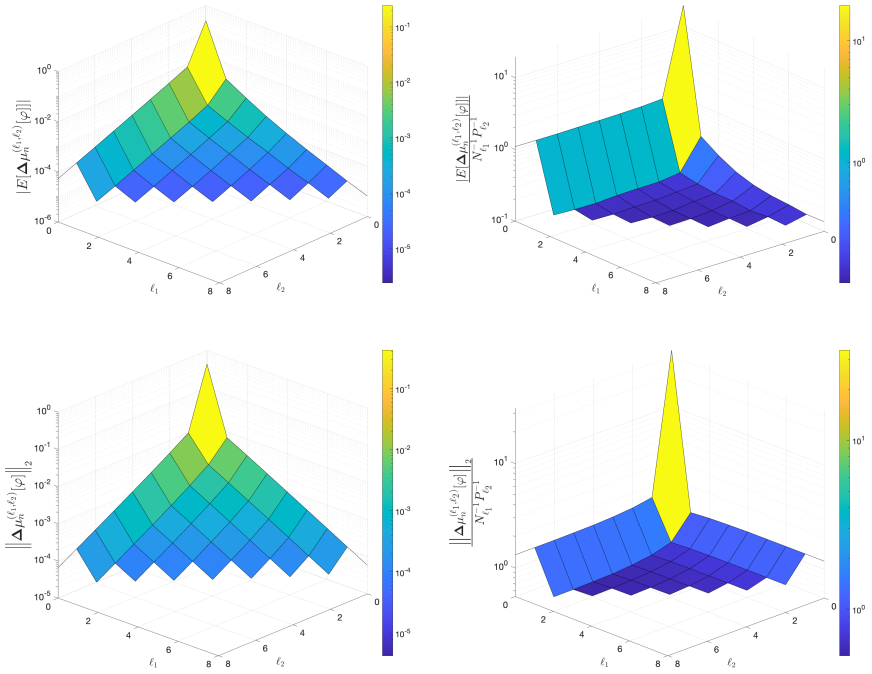
(Håkon Hoel)
Department of Mathematics, University of Oslo, Oslo, Norway
(haakonah@math.uio.no)

(Gaukhar Shaimerdenova)
Applied Mathematics and Computational Sciences, KAUST, Thuwal, Saudi Arabia
(gaukhar.shaimerdenova@kaust.edu.sa)

(Raul Tempone)
Chair of Mathematics for Uncertainty Quantification, RWTH Aachen University, Aachen, Germany
(tempone@uq.rwth-aachen.de)
and
Applied Mathematics and Computational Sciences, KAUST, Thuwal, Saudi Arabia
(raul.tempone@kaust.edu.sa)

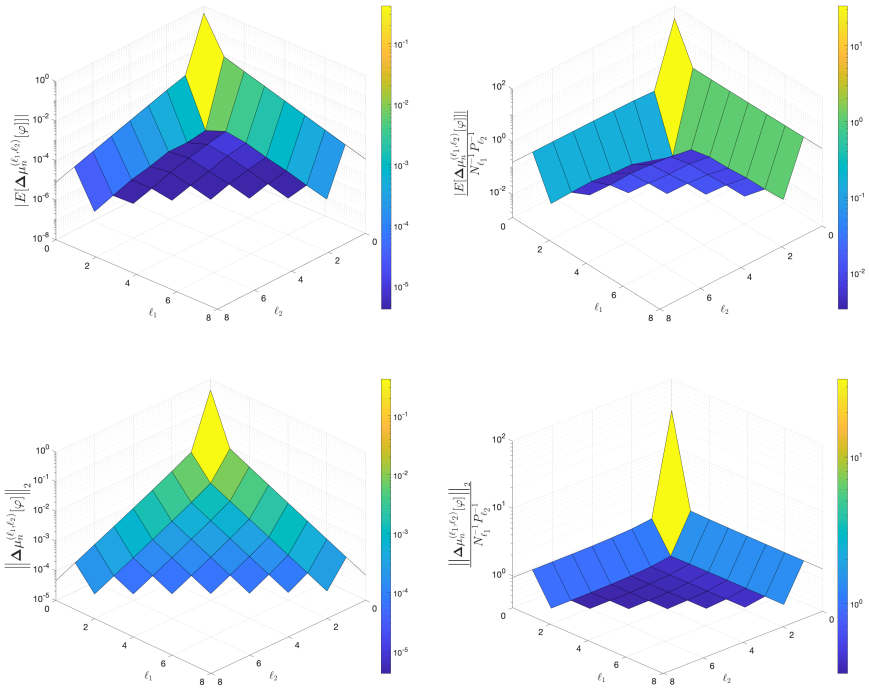


(a) The particle position X_t

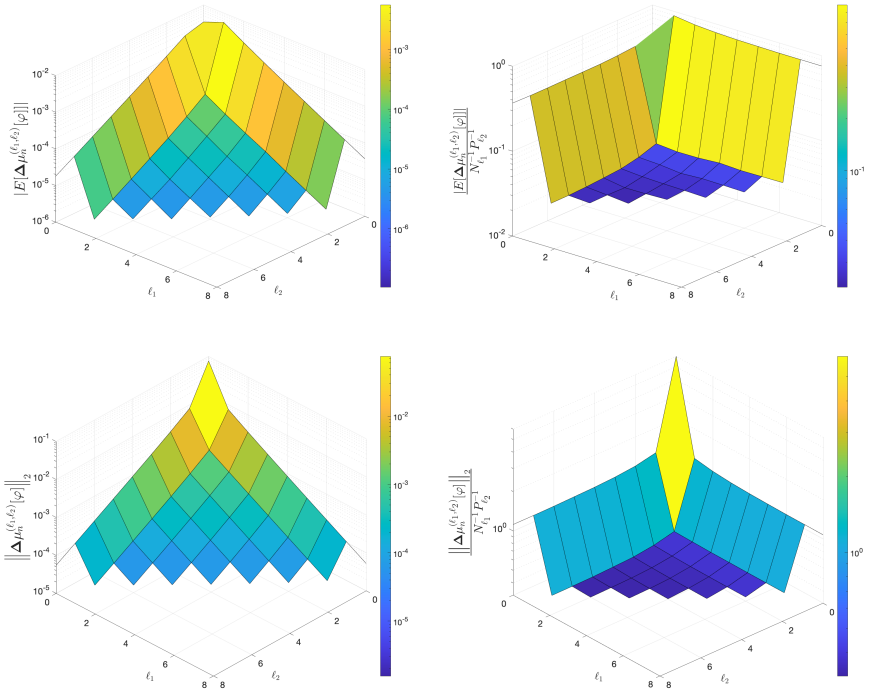


(b) The particle velocity V_t

FIGURE 8. **Langevin dynamics with partial observations, $H = [1\ 0]$. Estimates based on $S = 10^6$ independent runs (Section 5.4).** Top row in each subfigure: Numerical evidence of assumption (**A1**) for $\mathcal{N} = 10$ observation times when using $N_{\ell_1} = 4 \times 2^{\ell_1}$ and $P_{\ell_2} = 20 \times 2^{\ell_2}$. Bottom row in each subfigure: Similar plots for verifying assumption (**A2***).



(a) The particle position X_t



(b) The particle velocity P_t

FIGURE 9. **Langevin dynamics with full observations,** $H = [1\ 0; 0\ 1]$**. Estimates based on** $S = 10^6$ **independent runs (Section 5.4).** Similar plots as those shown in Figure 8.

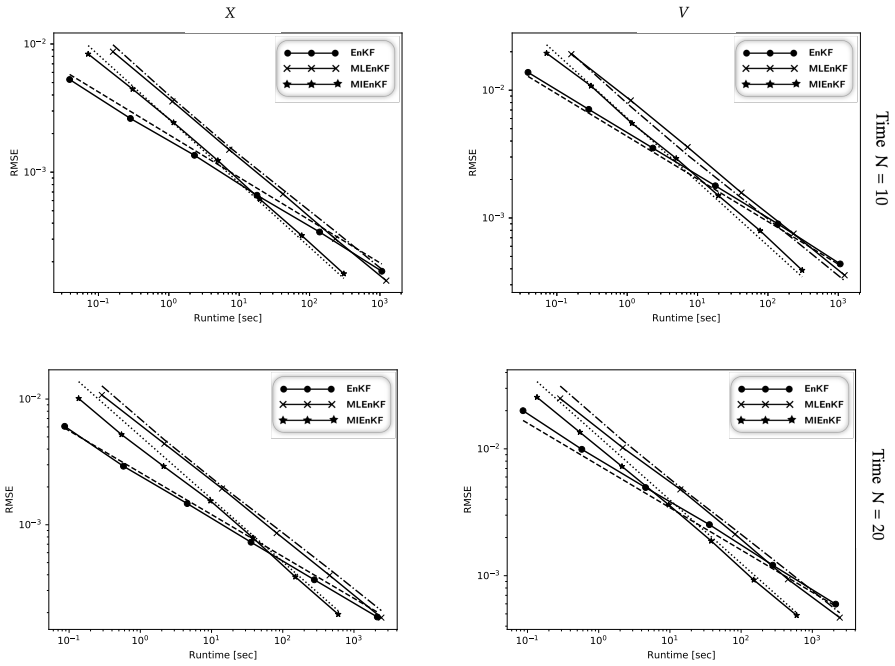


FIGURE 10. **Langevin dynamics with partial observations,** $H = [1\ 0]$**. Estimates based on** $S = 90$ **independent runs (Section 5.4).** *Top row*: Comparison of the runtime versus RMSE for the mean of the component X (left) and the component V (right) over $\mathcal{N} = 10$ observation times. The solid-crossed line represents MLEnKF and the dot-dashed line is a fitted $\mathcal{O}(\log(10 + \text{Runtime})^{1/3}\text{Runtime}^{-1/2})$ reference line. The solid-asterisk line represents the MIEnKF and the dotted line is a fitted $\mathcal{O}(\text{Runtime}^{-1/2})$ reference line. The solid-bulleted line represents EnKF and the dashed line is a fitted $\mathcal{O}(\text{Runtime}^{-1/3})$ reference line. *Bottom row*: Similar plots for $\mathcal{N} = 20$ observation times.

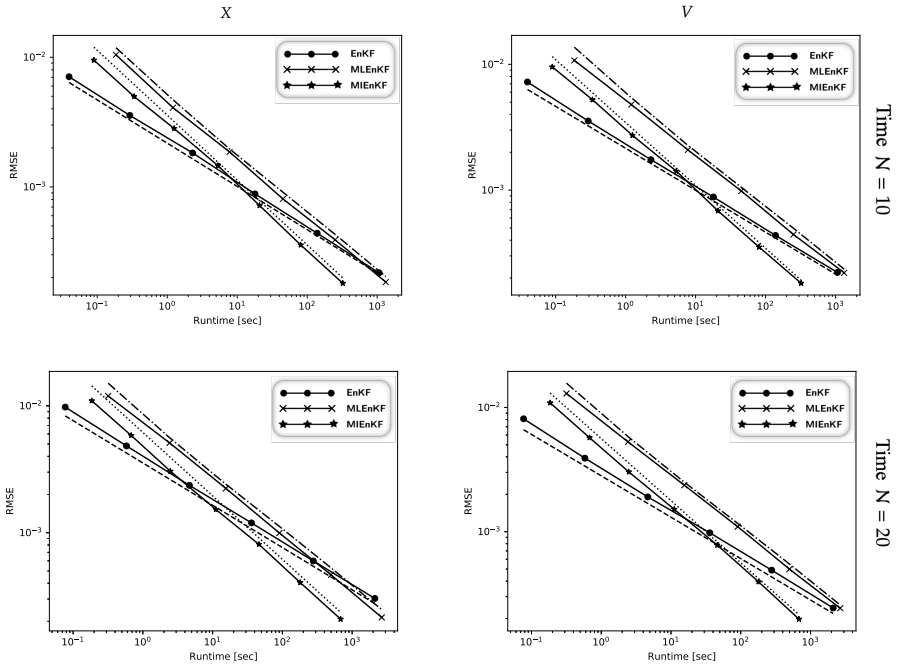


FIGURE 11. **Langevin dynamics with full observations, $H = [1\ 0; 0\ 1]$. Estimates based on $S = 90$ independent runs (Section 5.4).** Similar plots as those shown in Figure 10.